

NACA RM L53H14

7459

NACA

*Corrected
copy*

RESEARCH MEMORANDUM

AN ENGINEERING METHOD FOR THE DETERMINATION
OF AEROELASTIC EFFECTS UPON THE ROLLING EFFECTIVENESS OF
AILERONS ON SWEPT WINGS

By H. Kurt Strass and Emily W. Stephens

Langley Aeronautical Laboratory
Langley Field, Va.

Class.

By

By

GRADE C

NATIONAL ADVISORY COMMITTEE
FOR AERONAUTICS

WASHINGTON

November 30, 1953



NATIONAL ADVISORY COMMITTEE FOR AERONAUTICS

RESEARCH MEMORANDUM

AN ENGINEERING METHOD FOR THE DETERMINATION
OF AEROELASTIC EFFECTS UPON THE ROLLING EFFECTIVENESS OF
AILERONS ON SWEPT WINGS

By H. Kurt Strass and Emily W. Stephens

SUMMARY

A method is presented for calculating the steady-state rolling effectiveness of flexible sweptback wings at subsonic and supersonic speeds. The present method was derived by reducing the problem to its simplest terms. The result is a procedure which possibly is as simple as can be devised, and which, based on comparisons with experiment, apparently is still capable of providing estimates of the changes in aileron rolling effectiveness for a wide range of wing-aileron configurations within the experimental accuracy.

As an aid to rapid calculation, the results of this investigation are presented in nondimensional form and have been calculated for a wide range of tapered wings varying from 0 to 1.0 in taper ratio, for wing-span--body-diameter ratios of 0, 0.2, and 0.4, and for ailerons of any spanwise extent and location. These calculations were made assuming that the wings were of homogeneous construction. The direct application of the results of this investigation to wings wherein the structural parameters differ markedly from a homogeneous wing should be avoided. It is recommended in these cases that a closer approximation to the actual aerodynamic and structural values be used and a particular solution, also presented herein, be obtained.

Comparisons between the experimental and calculated values are presented for a wide range of wing-aileron configurations. An illustrative example is included to facilitate calculations by this method. In addition, some experimentally determined structural constants are compared with those calculated by approximate methods.

INTRODUCTION

In recent years, many methods have been proposed to account for the effects of aeroelasticity upon the lateral-control characteristics of swept wings. Because of the complicated interaction of structural and aerodynamic effects, the theories which have been developed are necessarily complex. Relatively simple methods for making such estimates for unswept wings at both subsonic and supersonic speeds are available; however, a comparable method for swept wings which does not involve the use of difficult mathematical procedures and which is relatively rapid and reasonably accurate has not been available. Such a method would be of particular importance in preliminary design.

In order to correlate the test results of the more than 370 successful lateral-control test models which have been flown by the Langley Pilotless Aircraft Research Division in the course of a general investigation of lateral control over a speed range which extended from approximately $M = 0.6$ to as high as $M = 1.8$, it was necessary to account for the effects of aeroelastic distortion. Because of the great number and variety of wing-control configurations, the application of a highly refined aeroelastic theory would have been exceedingly tedious. The purpose of this paper is to present the engineering method which was derived and the comparison of the values calculated by this method with experiment.

The results of this investigation for ailerons are presented in non-dimensional form and have been calculated for a range of tapered wings varying from 0 to 1.0 in taper ratio, for wing-span--body-diameter ratios of 0, 0.2, and 0.4 and for ailerons of any spanwise extent and location.

An example problem is outlined in appendix A. In addition, some experimentally determined structural constants are compared with those calculated by approximate methods. This comparison is given in appendix B.

SYMBOLS

AR aspect ratio, b^2/S

A dimensionless angle of twist resulting from the component of the aerodynamic moment parallel to the direction of flight caused by unit control deflection,

$$\int_{k_R}^k \frac{1}{\left(\frac{c}{\bar{c}}\right)^4} \left[\int_k^1 \left(\frac{c}{\bar{c}}\right)^2 dk \right] dk$$

CONFIDENTIAL

- B dimensionless angle of twist resulting from the component of the aerodynamic moment parallel to the direction of flight caused by rolling,
$$\int_{k_R}^k \frac{1}{\left(\frac{c}{c}\right)^4} \left[\int_k^1 \left(\frac{c}{c}\right)^2 k dk \right] dk$$
- C dimensionless angle of twist resulting from the component of the aerodynamic moment parallel to the elastic axis caused by unit control deflection,
$$\int_{k_R}^k \frac{1}{\left(\frac{c}{c}\right)^4} \left[\int_k^1 \frac{c}{c} (k_P - k_R) dk_P - (k - k_R) \int_k^1 \frac{c}{c} dk_P \right] dk$$
- D dimensional angle of twist resulting from the component of the aerodynamic moment parallel to the elastic axis caused by rolling,
$$\int_{k_R}^k \frac{1}{\left(\frac{c}{c}\right)^4} \left[\int_k^1 \frac{c}{c} k_P (k_P - k_R) dk_P - (k - k_R) \int_k^1 \frac{c}{c} k_P dk_P \right] dk$$
- E Young's modulus of elasticity, lb/sq in.
- G shear modulus of elasticity, lb/sq in.
- I moment of inertia of airfoil cross section about chord plane, in.⁴
- J torsional stiffness constant of airfoil cross section in plane parallel to the direction of flight, in.⁴
- K₁, K₂ proportionality constants
- L rolling moment (positive clockwise, as seen from the rear), in-lb
- M accumulated bending moment in a plane perpendicular to the elastic axis (positive when bending wing in clockwise direction, as seen from rear), in-lb
- M Mach number
- P distributed load, lb/in.

S	wing area, sq in.
T	accumulated twisting moment parallel to the direction of flight (positive when tending to twist wings in a direction to create positive change in section angle of attack), in-lb
V	velocity, ft/sec
b	wing span, in.
\bar{c}	mean wing chord, S/b , in.
c	wing chord, in.
d_1	distance of center of pressure of load due to angle of attack from elastic axis (positive forward), fraction of chord
d_2	distance of center of pressure of load due to control deflection from elastic axis (positive forward), fraction of chord
e	distance of elastic axis from leading edge, fraction of chord
k	distance to any point on the elastic axis, measured from fuselage center line, fraction of semispan, $\frac{x}{b/2}$
l	lift per unit length, lb/in.
p	rate of roll (positive when rolling in a clockwise direction, as seen from rear), radians/sec
q	dynamic pressure, lb/sq in.
t	maximum airfoil thickness, in.
$pb/2V$	wing tip helix angle due to unit aileron deflection (rolling effectiveness parameter), radians
c^4/GJ	nonscalar torsional stiffness parameter, in. ² /lb
δ	control-surface deflection, measured in a plane parallel to the direction of flight, positive when producing a clockwise rolling moment as seen from the rear, radians
λ	taper ratio, ratio of tip chord to chord at fuselage center line
β	slope of deflection curve, radians

- θ twist of wing about elastic axis, radians
- ϕ fraction of rigid wing rolling effectiveness retained by flexible wing
- α section angle-of-attack change due to aeroelastic deformation (positive when in direction to create positive rolling moment), radians
- Λ_e sweep of elastic axis, deg
- α_δ section control effectiveness parameter, effective change in wing angle of attack caused by unit change in control-surface deflection
- c_{l_α} section lift-curve slope, per radian
- C_{L_α} wing lift-curve slope, per radian
- $c_{l_\delta} = \frac{\partial c_l}{\partial \delta}$
- $c_{l_p} = \frac{\partial c_l}{\partial \frac{pb}{2V}}$
- C_l rolling-moment coefficient, L/qSb , positive clockwise when viewed from rear
- $(C_l)_f$ additional rolling-moment coefficient resulting from wing flexibility
- Subscripts:
- A,B,C,D particular types of aerodynamic loading resulting from structural deformation
- M signifies that value is for a bending moment parallel to the elastic axis
- P load
- R wing root, intersection of elastic axis and fuselage
- T signifies that value is for twisting moment parallel to the direction of flight

a	aileron
f	flexible wing
r	rigid wing
α	angle of attack
δ	control deflection
i	inboard
o	outboard
p	roll
1,2	arbitrary reference points

Prime marks denote that the reference plane is either normal to or parallel to the elastic axis rather than normal to or parallel to the direction of flight.

DEVELOPMENT OF EQUATIONS FOR THE DETERMINATION OF AEROELASTIC
EFFECTS UPON THE ROLLING EFFECTIVENESS
OF AILERONS ON SWEEPED WINGS

In a steady roll, the resultant rolling moment acting on a wing is zero. In coefficient form this can be expressed as follows for a flexible wing:

$$\delta C_{l\delta} + \left(\frac{pb}{2V}\right)_f C_{lp} + (C_l)_f = 0 \quad (1)$$

rewriting equation (1) gives

$$\left(\frac{pb}{2V}\right)_f = \frac{-\delta C_{l\delta} - (C_l)_f}{C_{lp}} \quad (2)$$

The fraction of control effectiveness lost by the wing is

$$(1 - \phi) = 1 - \frac{(pb/2V)_f}{(pb/2V)_r} = \frac{-(C_l)_f}{\delta C_{l\delta}} \quad (3)$$

For the purposes of this derivation, the following assumptions and definitions are used:

(1) The angles of twist parallel to the direction of flight resulting from the application of aerodynamic forces can be calculated by the use of the elementary theories of torsion and bending when correction is made for the effects of root restraint by a simple empirical method. This method assumes that the wing has an elastic axis and all the aerodynamic forces can be separated into loads which act on the elastic axis and couples which act about the elastic axis.

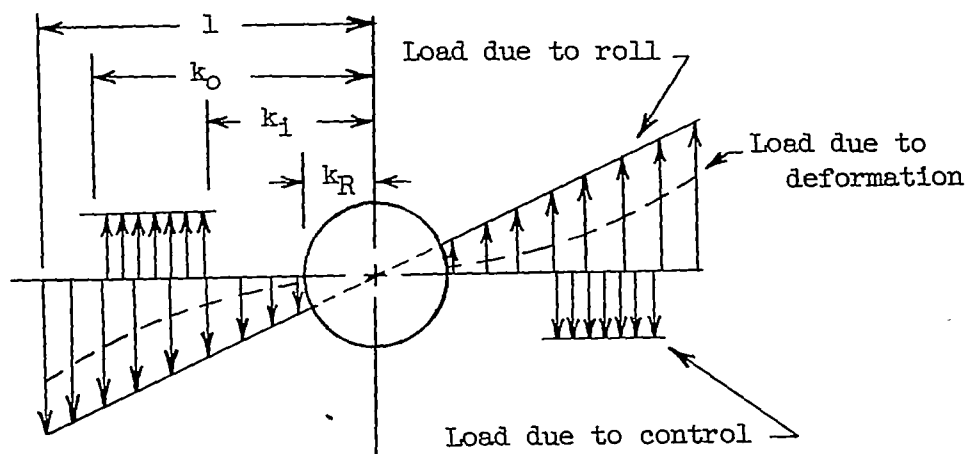
(2) The changes in rolling effectiveness due to aeroelastic effects are small in comparison with the rigid-wing values. The loads created by aeroelastic deformations are small in comparison with the loads created by rolling and aileron deflection.

(3) The control deflection is constant and is independent of aeroelastic effects.

(4) The chord of the wing varies linearly with the span.

(5) There is no yaw or sideslip.

(6) Within the framework of these assumptions, a schematic description of the spanwise variation of the aerodynamic loads for a typical wing with the control deflected is as follows:



where $k = \frac{x}{b/2}$. All the aeroelastic phenomena result from the application of these loads.

(7) The lift due to either control deflection or a change in angle of attack acts at the chordwise center of pressure. This assumption is equivalent to assuming that the wing sections are infinitely rigid and cannot distort (camber) under the distributed chordwise air loads.

(8) The incremental lift due to control deflection acts independently of the lift because of a change in angle of attack. The wing deformations resulting from these loads can be superimposed upon each other.

(9) The incremental loads at any station due to elastic deformation are dependent solely on the angle of attack at that station.

Structural Analysis

Within the limitations imposed by the first assumption, the angle of attack at any point along the span of a sweptback wing resulting from loads which act on the elastic axis and couples which act about the elastic axis can be derived as follows:

Angle of attack resulting from wing bending. - From elementary theory, the change in slope between any two points k_1' and k_2' on a wing (see fig. 1) due to the previously mentioned loading is

$$\left. \begin{aligned} \Delta\theta \Big|_{k_1'}^{k_2'} &= \frac{b'}{2} \int_{k_1'}^{k_2'} \frac{M dk'}{E'I'} \\ M &= M_P' + M_T' \end{aligned} \right\} \quad (4)$$

where

$$M = \frac{b'^2}{4} \int_{k'}^1 P'(k_P' - k') dk_P' + T'$$

thus

$$\Delta\beta \begin{bmatrix} k_2' \\ k_1' \end{bmatrix} = \frac{b'}{2} \int_{k_1'}^{k_2'} \frac{1}{E'I'} \left[\frac{b'^2}{4} \int_{k'}^1 P'(k_P' - k') dk_P' + T' \right] dk' \quad (5)$$

where

$$\Delta\beta \begin{bmatrix} k_2' \\ k_1' \end{bmatrix} = \Delta\alpha_M \begin{bmatrix} k_2 \\ k_1 \end{bmatrix} \frac{1}{\sin \Lambda_e}$$

$$k' = \frac{x'}{b'/2} = \frac{x}{b/2} = k$$

$$I' = I \cos \Lambda_e$$

$$E' = E$$

$$b' = \frac{b}{\cos \Lambda_e}$$

$$P' = P \cos \Lambda_e$$

$$T' = T \sin \Lambda_e$$

Substituting these values into equation (5) gives

$$\Delta\alpha_M \begin{bmatrix} k_2 \\ k_1 \end{bmatrix} = \frac{b}{2} \frac{\sin \Lambda_e}{\cos^2 \Lambda_e} \int_{k_1}^{k_2} \frac{1}{EI} \left[\frac{b^2}{4} \frac{1}{\cos \Lambda_e} \int_k^1 P(k_P - k) dk_P + T \sin \Lambda_e \right] dk \quad (6)$$

Angle of attack resulting from wing twisting about the elastic axis.-
From elementary theory, the change in the angle of twist about the elastic axis between any two points k_1' and k_2' on a wing due to the previously mentioned loading is

CONFIDENTIAL

$$\Delta\theta \Big|_{k_1'}^{k_2'} = \frac{b'}{2} \int_{k_1'}^{k_2'} \frac{T \cos \Lambda_e dk'}{G' J'} \quad (7)$$

where

$$\Delta\theta \Big|_{k_1'}^{k_2'} = \Delta\alpha_{T \cos \Lambda_e} \Big|_{k_1}^{k_2} \frac{1}{\cos \Lambda_e}$$

$$G' = G$$

$$J' = J \cos \Lambda_e$$

Substituting these values into equation (7) gives

$$\Delta\alpha_{T \cos \Lambda_e} \Big|_{k_1}^{k_2} = \frac{b}{2} \int_{k_1}^{k_2} \frac{T dk}{GJ} \quad (8)$$

For the purpose of this paper it is desirable to express the changes in angle of attack due to aeroelastic deformation as angular changes due to loads on the elastic axis and to twisting couples acting about an axis perpendicular to the direction of flight. Rewriting equation (6) as

$$\Delta\alpha_M \Big|_{k_1}^{k_2} = \Delta\alpha_P \Big|_{k_1}^{k_2} + \Delta\alpha_{T \sin \Lambda_e} \Big|_{k_1}^{k_2}$$

gives

$$\Delta\alpha_P \Big|_{k_1}^{k_2} = \Delta\alpha_M - \Delta\alpha_{T \sin \Lambda_e} = \frac{b^3}{8} \frac{\sin \Lambda_e}{\cos^3 \Lambda_e} \int_{k_1}^{k_2} \left[\frac{1}{EI} \int_{k_1}^1 P(k_P - k_1) dk_P \right] dk \quad (9)$$

Similarly from equations (6) and (8)

$$\begin{bmatrix} \Delta\alpha_T \\ \end{bmatrix}_{k_1}^{k_2} = \Delta\alpha_{T\sin\Lambda_e} \begin{bmatrix} \\ \end{bmatrix}_{k_1}^{k_2} + \Delta\alpha_{T\cos\Lambda_e} \begin{bmatrix} \\ \end{bmatrix}_{k_1}^{k_2}$$

so that

$$\begin{bmatrix} \Delta\alpha_T \\ \end{bmatrix}_{k_1}^{k_2} = \frac{b}{2} \left(\frac{\sin \Lambda_e}{\cos^2 \Lambda_e} \int_{k_1}^{k_2} \frac{T \sin \Lambda_e dk}{EI} + \int_{k_1}^{k_2} \frac{T dk}{GJ} \right)$$

which can be written as

$$\begin{bmatrix} \Delta\alpha_T \\ \end{bmatrix}_{k_1}^{k_2} = \frac{b}{2} \int_{k_1}^{k_2} \left(1 + \tan^2 \Lambda_e \frac{GJ}{EI} \right) \frac{T dk}{GJ} \quad (10)$$

In order that the foregoing beam theory give accurate results for swept wings it is necessary to take into account the effect of the triangular root portion. One way to do this is by making use of the so-called "effective root" concept (see ref. 1, for example). If the effective root is located at $k = k_R + \Delta k$ then the resulting expressions for the angle of attack at any point along the span due to the applied forces are

$$\alpha_P = \frac{b^3}{8} \frac{\sin \Lambda_e}{\cos^3 \Lambda_e} \int_{k_R + \Delta k}^k \frac{1}{EI} \left[\int_k^1 P(k_P - k) dk_P \right] dk \quad (11)$$

$$\alpha_T = \frac{b}{2} \int_{k_R + \Delta k}^k \left(1 + \tan^2 \Lambda_e \frac{GJ}{EI} \right) \frac{T dk}{GJ} \quad (12)$$

Aeroelastic Analysis

As a consequence of assumption 2 it is assumed that the distortions caused by the loads resulting from the distortions themselves are negligible. The only distortions considered are those caused by the aileron loads and the loads due to rolling. These distortions are denoted as follows:

- α_A the change in angle of attack caused by the torque resulting from aileron deflection
- α_B the change in angle of attack caused by the torque resulting from rolling
- α_C the change in angle of attack caused by the load on the elastic axis resulting from aileron deflection
- α_D the change in angle of attack caused by the load on the elastic axis resulting from rolling

The rolling-moment coefficients resulting from these distortions are denoted in a similar manner, C_{l_A} , C_{l_B} , C_{l_C} , and C_{l_D} .

Rolling-moment coefficients resulting from the elastic deformations caused by the aerodynamic twisting moments parallel to the direction of flight.

Effect of aileron deflection - see figure 2: At any point k the section twisting moment due to unit positive aileron deflection is

$$l_0 d_2 \frac{c}{c} \bar{c}$$

where the lift per unit length, due to unit control deflection, is

$$l_0 = qc l_{\alpha} \alpha_0 \frac{c}{c} \bar{c} \quad (13)$$

Therefore, the general expression for the twisting moment is

$$T_A = q \frac{b}{2} \bar{c}^2 \int_k^{k_0} d_2 \alpha_0 c l_{\alpha} \left(\frac{c}{c} \right)^2 dk \quad (14)$$

Specifically:

Region 1 (inboard of aileron)

$$T_A = q \frac{b}{2} \bar{c}^2 \int_{k_i}^{k_o} d_2 \alpha_0 c l_{\alpha} \left(\frac{c}{\bar{c}} \right)^2 dk \quad (15a)$$

Region 2 (in way of aileron)

$$T_A = q \frac{b}{2} \bar{c}^2 \int_k^{k_o} d_2 \alpha_0 c l_{\alpha} \left(\frac{c}{\bar{c}} \right)^2 dk \quad (15b)$$

Region 3 (outboard of aileron)

$$T_A = 0 \quad (15c)$$

Substituting T_A into equation (12) gives the angle of attack at any point on a sweptback wing due to the twisting moment created by the aileron deflection.

$$\alpha_A = q \frac{b \bar{c}^2}{4} \int_{k_R + \Delta k}^k \frac{1 + \tan^2 \Lambda_e \frac{GJ}{EI}}{GJ} \left[\int^* d_2 \alpha_0 c l_{\alpha} \left(\frac{c}{\bar{c}} \right)^2 dk \right] dk \quad (16)$$

where

$$\int^* = \int_{k_i}^{k_o} \quad (\text{in region 1})$$

$$= \int_k^{k_o} \quad (\text{in region 2})$$

$$= \int_{k_o}^1 = 0 \quad (\text{in region 3})$$

The rolling-moment coefficient due to the spanwise distribution of α_{TA} is

$$C_{LA} = \frac{L_{TA}}{qSb} = \frac{2q \frac{b^2}{4} \bar{c} \int_{k_R+\Delta k}^1 \alpha_{TA} c_{l_\alpha} \frac{c}{\bar{c}} k dk}{qSb} \quad (17)$$

Substituting for α_{TA} in equation (17) and simplifying gives

$$C_{LA} = q \frac{S^2}{8} \int_{k_R+\Delta k}^1 c_{l_\alpha} \frac{c}{\bar{c}} k \left\{ \int_{k_R+\Delta k}^k \frac{1 + \tan^2 \Lambda_e \frac{GJ}{EI}}{GJ} \left[\int^* d_2 \alpha_0 c_{l_\alpha} \left(\frac{c}{\bar{c}} \right)^2 dk \right] dk \right\} dk \quad (18)$$

Effect of rolling: At any point k the section twisting moment due to roll is

$$l_p d_1 \frac{c}{\bar{c}} \bar{c}$$

where the lift per unit length resulting from the roll caused by unit aileron deflection is

$$l_p = -\bar{c} q \frac{c}{\bar{c}} c_{l_\alpha} k \frac{pb}{2V} \quad (19)$$

(the negative sign indicates that the lift due to roll is opposite to the lift due to control deflection).

$$T_B = -q \frac{b}{2} \bar{c}^2 \frac{pb}{2V} \int_k^1 d_1 c_{l_\alpha} \left(\frac{c}{\bar{c}} \right)^2 k dk \quad (20)$$

and in a manner similar to that used previously, the angle of twist at any point on a sweptback wing due to the twisting moment created by rolling is

$$\alpha_B = -q \frac{b^2 \bar{c}^2}{4} \frac{pb}{2V} \int_{k_R + \Delta k}^k \left(\frac{1 + \tan^2 \Lambda_e \frac{GJ}{EI}}{GJ} \right) \left[\int_k^1 d_1 c_{l_\alpha} \left(\frac{c}{\bar{c}} \right)^2 k dk \right] dk \quad (21)$$

and the rolling-moment coefficient is

$$C_{l_B} = -q \frac{s^2}{8} \frac{pb}{2V} \int_{k_R + \Delta k}^1 c_{l_\alpha} \frac{c}{\bar{c}} k \left\{ \int_{k_R + \Delta k}^k \frac{1 + \tan^2 \Lambda_e \frac{GJ}{EI}}{GJ} \left[\int_k^1 d_1 c_{l_\alpha} \left(\frac{c}{\bar{c}} \right)^2 k dk \right] dk \right\} dk \quad (22)$$

Rolling-moment coefficients resulting from the elastic deformations caused by the aerodynamic loads on the elastic axis.-

Effect of aileron deflection: The load P for a unit aileron deflection is

$$P = 0 \quad (k < k_1)$$

$$P = l_\delta = qc_{l_\alpha} \alpha_\delta \left(\frac{c}{\bar{c}} \right) \bar{c} \quad (k_1 < k < k_0)$$

$$P = 0 \quad (k > k_0)$$

Substituting for P into equation (11) gives the angle of attack at any point k caused by the loads resulting from the aileron deflection. The angle of attack anywhere on a sweptback wing due to the loads

on the elastic axis created by a positive aileron deflection is obtained by substituting the expression for M_C into equation (11).

$$\alpha_C = -q \frac{b^3 \bar{c}}{8} \frac{\sin \Lambda_e}{\cos^3 \Lambda_e} \int_{k_R + \Delta k}^k \frac{1}{EI} \left(\int^* \alpha_6 c_{l_\alpha} \frac{c}{c} k_P dk_P - k \int^* \alpha_6 c_{l_\alpha} \frac{c}{c} k_P dk_P \right) dk \quad (23)$$

The rolling-moment coefficient resulting from the wing bending caused by the aileron is

$$C_{LC} = -q \frac{S^2_{AR}}{16} \frac{\sin \Lambda_e}{\cos^3 \Lambda_e} \int_{k_R + \Delta k}^1 c_{l_\alpha} \frac{c}{c} k \left[\int_{k_R + \Delta k}^k \frac{1}{EI} \left(\int^* \alpha_6 c_{l_\alpha} \frac{c}{c} k_P dk_P - k \int^* \alpha_6 c_{l_\alpha} \frac{c}{c} k_P dk_P \right) dk \right] dk \quad (24)$$

Effect of rolling: For the rolling case, the load P is equivalent to the lift per unit length of span on the elastic axis resulting from the rolling due to unit aileron deflection.

$$P = l_P = -q c_{l_\alpha} \frac{c}{c} \bar{c} k_P \frac{pb}{2V}$$

The angle of attack anywhere on the sweptback wing is

$$\alpha_D = q \frac{b^3 \bar{c}}{8} \frac{\sin \Lambda_e}{\cos^3 \Lambda_e} \frac{pb}{2V} \int_{k_R + \Delta k}^k \frac{1}{EI} \left(\int_k^1 c_{l_\alpha} \frac{c}{c} k_P^2 dk_P - k \int_k^1 c_{l_\alpha} \frac{c}{c} k_P dk_P \right) dk \quad (25)$$

and the rolling-moment coefficient resulting from the wing bending caused by rolling is

$$C_{l_D} = q \frac{pb}{2V} \frac{S^2 AR}{16} \frac{\sin \Lambda_e}{\cos^3 \Lambda_e} \int_{k_R + \Delta k}^1 c_{l_\alpha} \frac{c}{c} k \left[\int_{k_R + \Delta k}^k \frac{1}{EI} \left(\int_k^1 c_{l_\alpha} \frac{c}{c} k_P^2 dk_P - \right. \right. \\ \left. \left. k \int_k^1 c_{l_\alpha} \frac{c}{c} k_P dk_P \right) dk \right] dk \quad (26)$$

Rolling-moment coefficient due to unit control deflection.-

$$C_{l_\delta} = \frac{I_\delta}{qSb} = \frac{2q \frac{b^2}{4} \int_{k_1}^{k_0} \alpha_\delta c_{l_\alpha} \frac{c}{c} k dk}{qSb} = \frac{1}{2} \int_{k_1}^{k_0} \alpha_\delta c_{l_\alpha} \frac{c}{c} k dk \quad (27)$$

Loss in rolling effectiveness due to aeroelasticity.- From equation (3)

$$1 - \phi = \frac{-(C_l)_F}{\delta C_{l_\delta}} \quad (\delta = 1)$$

where

$$(C_l)_F = C_{l_A} + C_{l_B} + C_{l_C} + C_{l_D}$$

$$1 - \phi = - \frac{[(eq. (18)) + (eq. (22)) + (eq. (24)) + (eq. (26))]}{(eq. (27))} \quad (28)$$

Appreciable simplification of equation (28) can be accomplished if certain additional qualifying assumptions can be made.

These assumptions are:

(10) The wing acts structurally as if it were of homogeneous construction and constant thickness ratio; that is, the structural parameters EI and GJ vary as the fourth power of the wing chord.

(11) The lift-curve slope is constant along the wing span and is equal to the value for the wing taken as a whole ($c_{l\alpha} = C_{L\alpha}$).

(12) The ratio of the aileron chord to wing chord is constant along the wing span (α_8 assumed constant).

(13) The distances d_1 and d_2 are constant.

According to the work done by Zender and Brooks and published in reference 1, a good approximation to the effective root for an homogeneous wing should be considered to be a point located on the elastic axis where a line drawn perpendicular to the elastic axis passes through the intersection of the wing trailing edge and the fuselage wall (see fig. 1). The spanwise location of this point can be expressed as

$$\Delta k = \frac{4}{AR(1 + \lambda)} \left\{ \left[(1 - e) \cos \Lambda_e \sin \Lambda_e \right] \left[1 - k_R(1 - \lambda) \right] \right\} \quad (29)$$

Reference 2 (page 171) gives the following expression (altered to conform to the symbols used in the present derivation) for the torsional constant for homogeneous sections similar to airfoils

$$J = \frac{4I}{1 + 16 \frac{I}{ac^2}} \quad (30)$$

where

a = cross-section area

$$I = K_1 ct^3 = K_1 c^4 \left(\frac{t}{c} \right)^3$$

$$a = K_2(tc)$$

$$\frac{16I}{ac^2} = \frac{16K_1 t^3 c}{K_2 t c^3} = 16 \frac{K_1}{K_2} \left(\frac{t}{c}\right)^2$$

$$J = 4I \frac{1}{1 + 16 \frac{K_1}{K_2} \left(\frac{t}{c}\right)^2}$$

For NACA 65AOXX airfoil sections

$$K_1 = 0.0377$$

$$K_2 = 0.651$$

If

$$\frac{t}{c} \rightarrow 0$$

then

$$J \rightarrow 4I \quad (31)$$

The error involved in this approximation is small for thin wings. By the use of the simplifying factors equation (16) can be rewritten in the following form:

$$\alpha_A = \frac{qb^2 d_2 \alpha_8}{16GK_1 c^2 \left(\frac{t}{c}\right)^3} C_{L\alpha} \left(1 + \tan^2 \Lambda_e \frac{GJ}{EI}\right) \left\{ \int_{k_R + \Delta k}^k \frac{1}{\left(\frac{c}{c}\right)^4} \left[\int^* \left(\frac{c}{c}\right)^2 dk \right] dk \right\} \quad (32)$$

Let the integral expression

$$\int_{k_R}^k \frac{1}{\left(\frac{c}{c}\right)^4} \left[\int^* \left(\frac{c}{c}\right)^2 dk \right] dk = A \quad (33)$$

$$\int_{k_R}^{k_R+\Delta k} \frac{1}{\left(\frac{c}{c}\right)^4} \left[\int^* \left(\frac{c}{c}\right)^2 dk \right] dk = \Delta A \quad (34)$$

then equation (32) can be simplified and rewritten in nondimensional form as

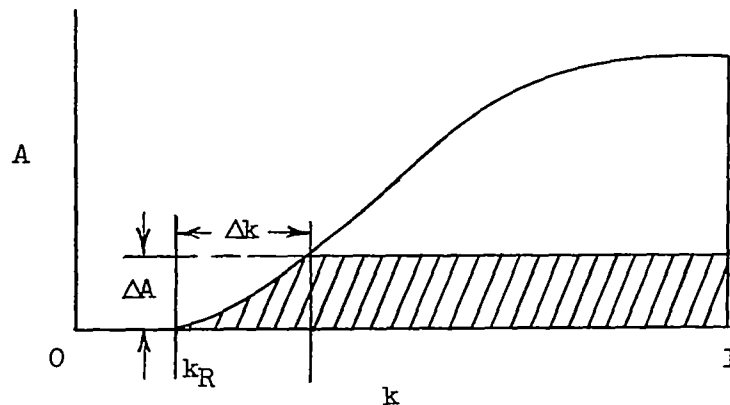
$$\alpha_A = \frac{q d_2 \alpha_6 C_{L\alpha}}{4} AR^2 \frac{c^4}{GJ} \left(1 + \tan^2 \Lambda_e \frac{GJ}{EI} \right) (A - \Delta A) \quad (35)$$

and

$$C_{L_A} = \frac{q d_2 \alpha_6 C_{L\alpha}^2}{8} AR^2 \frac{c^4}{GJ} \left(1 + \tan^2 \Lambda_e \frac{GJ}{EI} \right) \left[\int_{k_R}^1 A \frac{c}{c} k dk - \left(\int_{k_R}^{k_R+\Delta k} A \frac{c}{c} k dk + \int_{k_R+\Delta k}^1 \Delta A \frac{c}{c} k dk \right) \right] \quad (36)$$

The work necessary to evaluate equation (36) can be shortened appreciably by approximating the effect of the root restraint.

A typical variation of the function A with the spanwise coordinate k is presented in the following sketch



for which

$$\int_{k_R}^{k_R+\Delta k} A \frac{c}{\bar{c}} k \, dk + \int_{k_R+\Delta k}^1 \Delta A \frac{c}{\bar{c}} k \, dk = \text{area of shaded portion}$$

$$\approx \Delta A \int_{k_R+\frac{\Delta k}{2}}^1 \frac{c}{\bar{c}} k \, dk \quad (37)$$

Now

$$\frac{c}{\bar{c}} = \frac{2}{1+\lambda} [1 - k(1-\lambda)]$$

Substituting for c/\bar{c} in equation (32) and integrating gives

$$\Delta A \int_{k_R+\frac{\Delta k}{2}}^1 \frac{c}{\bar{c}} k \, dk = \frac{\Delta A}{3(1+\lambda)} \left\{ 3 \left[1 - \left(k_R + \frac{\Delta k}{2} \right)^2 \right] - \right.$$

$$\left. 2(1-\lambda) \left[1 - \left(k_R + \frac{\Delta k}{2} \right)^3 \right] \right\} \quad (38)$$

For convenience in usage, the expression for $\int_{k_R+\frac{\Delta k}{2}}^1 \frac{c}{\bar{c}} k \, dk$ has been calculated for several values of k_R , λ , and Δk and the values are presented in figure 3.

Substituting equation (38) into equation (36) gives the complete equation for the rolling-moment coefficient due to the twisting moment of the aileron.

CONFIDENTIAL

CONFIDENTIAL

$$C_{l_A} = \frac{q d_2^2 C_{l_\alpha}^2}{8} AR^2 \frac{c^4}{GJ} \left(1 + \tan^2 \Lambda_e \frac{GJ}{EI} \right) \left(\int_{k_R}^1 A \frac{c}{c} k dk - \Delta A \int_{k_R + \frac{\Delta k}{2}}^1 \frac{c}{c} k dk \right) \quad (39)$$

Values for $\int_{k_R}^1 A \frac{c}{c} k dk$ for $k_R = 0, 0.2$, and 0.4 are presented in figure 4. The root correction factor Δk can be obtained from equation (29). Figure 5 presents values of $\Delta A / \Delta k$ for root locations of $k_R = 0, 0.2$, and 0.4 . Then

$$\Delta A = \frac{\Delta A}{\Delta k} \Delta k$$

similarly equation (22) can be written

$$C_{l_B} = \frac{-q d_1 C_{l_\alpha}^2 AR^2}{8} \frac{pb}{2V} \frac{c^4}{GJ} \left(1 + \tan^2 \Lambda_e \frac{GJ}{EI} \right) \left(\int_{k_R}^1 B \frac{c}{c} k dk - \Delta B \int_{k_R + \frac{\Delta k}{2}}^1 \frac{c}{c} k dk \right) \quad (40)$$

where

$$B = \int_{k_R}^k \frac{1}{\left(\frac{c}{c}\right)^4} \left[\int_k^1 \left(\frac{c}{c}\right)^2 k dk \right] dk \quad (41)$$

The values for $\int_{k_R}^1 B \frac{c}{c} k dk$ can be obtained from figure 6, those for

$\Delta B / \Delta k$ from figure 7, and those for $\int_{k_R + \frac{\Delta k}{2}}^1 \frac{c}{c} k dk$, as for the previous

CONFIDENTIAL

case, from figure 3. Equation (24) can be written

$$C_{lC} = \frac{-q\alpha_0 C_{l\alpha}^2 AR^3}{16} \frac{c^4}{GJ} \frac{GJ}{EI} \frac{\sin \Lambda_e}{\cos^3 \Lambda_e} \left(\int_{k_R}^1 C \frac{c}{c} k dk - \Delta C \int_{k_R + \frac{\Delta k}{2}}^1 \frac{c}{c} k dk \right) \quad (42)$$

where

$$C = \int_{k_R}^k \frac{1}{\left(\frac{c}{c}\right)^4} \left(\int_{k_P}^* \frac{c}{c} k_P dk_P - k \int_{k_P}^* \frac{c}{c} dk_P \right) dk \quad (43)$$

The values for $\int_{k_R}^1 C \frac{c}{c} k dk$ can be obtained from figure 8, those for

$\Delta C / \Delta k$ from figure 9, and those for $\int_{k_R + \frac{\Delta k}{2}}^1 \frac{c}{c} k dk$ from figure 3. Equation (26) can be written

$$C_{lD} = q \frac{pb}{2V} \frac{C_{l\alpha}^2 AR^3}{16} \frac{c^4}{GJ} \frac{\sin \Lambda_e}{\cos^3 \Lambda_e} \frac{GJ}{EI} \left(\int_{k_R}^1 D \frac{c}{c} k dk - \Delta D \int_{k_R + \frac{\Delta k}{2}}^1 \frac{c}{c} k dk \right) \quad (44)$$

where

$$D = \int_{k_R}^k \frac{1}{\left(\frac{c}{c}\right)^4} \left(\int_k^1 \frac{c}{c} k_P^2 dk_P - k \int_k^1 \frac{c}{c} k_P dk_P \right) dk \quad (45)$$

The values for $\int_{k_R}^1 D \frac{c}{c} k dk$ can be obtained from figure 6, those for $\Delta D/\Delta k$ from figure 7, and those for $\int_{k_R + \frac{\Delta k}{2}}^1 \frac{c}{c} k dk$ from figure 3. Equation (27) can be rewritten

$$C_{l\delta} = \frac{\alpha_\delta C_{L\alpha}}{2} \int_{k_1}^{k_0} \frac{c}{c} k dk \quad (46)$$

Substituting the expression for c/\bar{c} into equation (46) and writing in general terms gives

$$C_{l\delta} = \frac{\alpha_\delta C_{L\alpha}}{6(1 + \lambda)} \left[3(k_0^2 - k_1^2) - 2(1 - \lambda)(k_0^3 - k_1^3) \right] \quad (47)$$

For convenience in usage, the terms which are dependent upon the wing-control geometry can be grouped together as follows:

$$\frac{C_{l\delta}}{\alpha_\delta C_{L\alpha}} = \frac{3(k_0^2 - k_1^2) - 2(1 - \lambda)(k_0^3 - k_1^3)}{6(1 + \lambda)} \quad (48)$$

Values for equation (48) are presented in figure 10, then

$$C_{l\delta} = \alpha_\delta C_{L\alpha} \left(\frac{C_{l\delta}}{\alpha_\delta C_{L\alpha}} \right)$$

Substituting the simplified expressions for equations (18), (22), (24), (26), and (27) into equation (28) gives

$$\begin{aligned}
 1 - \phi = & \frac{-q C_{L\alpha}^2 A R^2}{8 C_{l\delta}} \frac{c^4}{GJ} \left\{ \left[\left(1 + \tan^2 \Lambda_e \frac{GJ}{EI} \right) \left(d_2 \alpha_\delta \int_{k_R}^1 A \frac{c}{c} k dk - \right. \right. \right. \\
 & d_1 \frac{pb}{2V} \int_{k_R}^1 B \frac{c}{c} k dk \left. \right) - \frac{AR}{2} \frac{GJ}{EI} \frac{\sin \Lambda_e}{\cos^3 \Lambda_e} \left(\alpha_\delta \int_{k_R}^1 C \frac{c}{c} k dk - \right. \\
 & \left. \left. \frac{pb}{2V} \int_{k_R}^1 D \frac{c}{c} k dk \right) \right] - \int_{k_R + \frac{\Delta k}{2}}^1 \frac{c}{c} k dk \left[\left(1 + \tan^2 \Lambda_e \frac{GJ}{EI} \right) \left(d_2 \alpha_\delta \Delta A - \right. \right. \\
 & \left. \left. d_1 \frac{pb}{2V} \Delta B \right) - \frac{AR}{2} \frac{GJ}{EI} \frac{\sin \Lambda_e}{\cos^3 \Lambda_e} \left(\alpha_\delta \Delta C - \frac{pb}{2V} \Delta D \right) \right] \right\} \quad (49)
 \end{aligned}$$

Equation (49) is particularly suited to the estimation of the change in control effectiveness due to aeroelastic effects upon the free-flight lateral-control test models flown by the Pilotless Aircraft Research Division. An example application is made in appendix A. For many purposes, particularly in preliminary design, equation (49) can be used without modification. However, if more precise estimates are required, it is recommended that equation (28) be used.

APPLICATION AND COMPARISON WITH EXPERIMENT

Selection of Pertinent Parameters

In applying the simplified method to these cases, no attempt was made to determine the detailed aerodynamic parameters for a given wing-control configuration. For example, unswept two-dimensional wind-tunnel values of the control effectiveness parameter α_δ , the chordwise location of the center of lift due to angle of attack d_1 , and the chordwise location of the center of lift due to flap deflection d_2 were used throughout the calculations. The lift-curve slope $C_{L\alpha}$ was estimated from finite aspect-ratio wind-tunnel tests of wings of similar plan form and

thickness ratio in symmetrical lift. The restrictions resulting from these broad assumptions are obvious. The accuracy of estimation is a direct function of how well the aerodynamic values resulting from these assumptions approximate the actual conditions.

Another possible source of error results from the fact that many of the test wings were built up of wood and metal in various combinations and this form of construction has proved to be subject to relatively large variations in stiffness which are difficult to assess theoretically. (The only structural values which were obtained entirely from experimental data were the unswept wings; that is, Cases 1-8.) In addition, the method of attachment of the wings to the fuselage is not the ideal situation visualized by Zender and Brooks in reference 1, so that additional uncertainties exist. For example, some of the test wings were so stiff that comparatively large root deflections were experienced resulting in an appreciable reduction in root restraint. This movement of the wing root existed in all the test models. Its relative importance decreased as the wing stiffness decreased. In order to account for this factor, the effective root location was determined from experimental data wherever possible. It was observed that Zender and Brook's approximate root location became increasingly accurate as the wing stiffness relative to the stiffness of the fuselage was decreased.

Comparison of Simplified Method With Experiment

The effect of aeroelasticity upon the lateral control effectiveness as determined experimentally is compared with that estimated by the simplified method in figures 11 to 19. All of the data obtained to date have been included, with the exception of three cases wherein unusually large constructional errors were measured and for which proper allowance would have been virtually impossible without more detailed measurements.

The estimated effect of aeroelasticity is obtained as a fraction of the rigid-wing value; therefore, in order to obtain the actual value of the rolling effectiveness it is necessary that rigid-wing values be obtained. From equation (3)

$$\left(\frac{pb}{2V}\right)_r = \frac{(pb/2V)_f}{\phi}$$

The rigid-wing estimates which are presented were based upon the test data which, according to the method of estimation, were the least affected by aeroelasticity in order to obtain rigid-wing values of maximum accuracy. These estimated rigid-wing values were then used in the calculation of the flexible-wing values. A major assumption of the method

of estimation is that the changes in rolling effectiveness due to aeroelasticity are small in comparison with the rigid-wing values. However, comparisons between the experimental and estimated values are presented for cases where the changes in $pb/2V$ due to aeroelasticity exceed the estimated rigid-wing values. It is impossible to draw a line where the method is applicable and where it is not. The conditions would vary widely with structural and aerodynamic changes. These comparisons are presented for their own intrinsic value and are intended as a guide to the possible use of this method for design purposes.

All the data, except those presented in figures 16 and 17, have been corrected to a common aileron deflection of 5° parallel to the direction of flight. The data presented in figures 16 and 17 are corrected to common aileron angles of 5° and 10° , respectively, measured normal to the aileron hinge axis. All the data have been corrected to 0° wing incidence by the method given in reference 3. No other corrections have been applied. The data presented are for the altitude of the test, which varies continuously throughout the speed range. The variation of static pressure with Mach number can be obtained from the referenced papers if desired.

The geometrical characteristics of the test wings and the references from which the data for these wings were taken are given in table I. The structural and aerodynamic parameters used in the calculations are presented in tables II and III, respectively.

Figure 11 presents a comparison of the experimental results with the calculated values for a group of unswept, untapered wings. It should be noted that for the majority of the cases the estimated values agree very well with the measured values, with the exception of cases 2 and 8 for which the measured effect of aeroelasticity differs appreciably from that estimated. In consideration of the excellent agreement between estimate and experiment in the same speed range for the other cases in this group, it appears that some unknown model characteristics were responsible for the discrepancy. For example, cases 5 and 8 were nominally identical. The wings were constructed of laminated white pine. The nondimensional torsional stiffness constant for c^4/GJ as obtained from measured data for case 8 was only 4 percent greater than for case 5, yet the measured change in $pb/2V$ was 67 percent greater for case 8 as compared with case 5. Because the wings were constructed of wood, the probability that the wings warped after they had been measured is very great. Normally every effort is made to minimize the time between model measurement and flight test in order to avoid this and other troubles. However, experience has shown that the test data from the more flexible built-up wings wherein the wood was the primary load carrying material are definitely more subject to these indeterminate deviations.

Cases 1 and 2, being constructed of solid metal alloy, are not suspected of any dimensional change after model measurement. Because only two 3-percent-wing models were flown, it is not possible to draw any conclusions as to which of the cases is the probable aberrant one.

A group of untapered wings swept back 45° is presented in figure 12. As before, the most flexible case (case 13), which was also constructed of white pine, deviated the farthest from the estimated values. The remainder of the cases agreed with the estimates within the estimated experimental accuracy.

An interesting point is illustrated here in that the method of estimation indicates that for certain combinations of structural and aerodynamic values, the flexible values are higher than the rigid ones. This situation results from the fact that for these cases, the loss in damping moment due to roll is greater than the loss in rolling moment due to control deflection. If

$$\Delta I_{P_f} > \Delta I_{\delta_f}$$

and

$$(I_{\delta_r} - \Delta I_{\delta_f} + \Delta I_{P_f}) > I_{\delta_r}$$

then

$$\left(\frac{pb}{2V}\right)_f > \left(\frac{pb}{2V}\right)_r$$

It is to be remembered that the reduction of available control rolling moment because of aeroelastic effects seriously affects the time required to attain a given angle of bank even though the resultant steady-state value of $pb/2V$ may be higher than the rigid value.

In figure 13, for example, the flexible values are considerably higher than the estimated rigid values. The magnitude of the relieving effect of roll on the aeroelastic effects is very well illustrated by comparison of the experimental results for cases 16 and 17 (fig. 13(b)). In this particular instance, the wings of case 17 were approximately $1/7$

as stiff as case 16, yet there was no measurable difference between the two cases up to $M = 0.9$. At $M = 1.0$, the relieving effect of roll only partially overcame the large loss in control rolling moment, the net loss being approximately one-third of the rigid wing $pb/2V$.

No attempt was made to estimate the aeroelastic effects beyond $M = 1.0$ because the very unusual aerodynamic behavior of this group of models in this region indicates that the application of simplified aerodynamics would obviously be unrealistic. The determination of the probable aerodynamic loading is beyond the scope of this paper.

The effect of spanwise aileron location upon the aeroelastic behavior of a given wing is presented in figure 14. The loss due to aeroelasticity is greatest when the aileron load is concentrated near the wing tip as in figure 14(b), and least when the aileron load is concentrated near the root as in figure 14(c). The agreement between the experimental and calculated values is good for the cases presented in figures 14(a) and 14(b) and poor for the cases of figure 14(c). The poor agreement in figure 14(c) may be due to the fact that strip theory underestimates the effectiveness of the inboard ailerons and overestimates the effect of roll, thus exaggerating the errors inherent in this method.

Some additional comparisons between the experimental and calculated effects of aeroelasticity for more or less conventional aileron locations (that is, outboard partial-span ailerons) are presented in figures 15 to 18. In general, the agreement is within the estimated experimental error. A few of the cases are worthy of special mention, among them are cases 29, 31, and 33, which were constructed in such a manner as to duplicate as closely as possible the structural characteristics of actual aircraft. The fact that the agreement of the calculated values with the experimental is fairly good for these obviously practical cases is encouraging.

The data presented in figure 18 represent an extreme case as far as the applicability of this method of estimation is concerned. The effects of minor variables are greatly magnified. For example, the spread between case 34 (solid steel) and case 35 (solid aluminum alloy) is apparently almost entirely due to an unintentional built-in wing twist which created a load opposing that due to roll. The wing twist was approximately linear and the average for the three wings was approximately 0.4° at the wing tip measured parallel to the direction of flight. At $M = 1.2$, the estimated effect of this twist was to reduce the rolling effectiveness of the aluminum wing by 40 percent. It should be pointed out that the incidence correction normally used is a "rigid" wing correction and is an entirely separate consideration (see ref. 3).

In order to show the probable range of application of the simplified method, a comparison of the measured changes in rolling effectiveness due

to aeroelasticity with the calculated changes is presented in figure 19. Most of the cases are either within or very close to the estimated limits of accuracy. This estimated limit of accuracy is an average value obtained from past experience and represents the expected degree of repeatability of two supposedly identical test models. It should be noted that a high proportion of the cases which do not correlate within the estimated experimental error are cases wherein the measured changes in $pb/2V$ due to aeroelasticity exceeded an arbitrarily chosen value of 80 percent of the estimated rigid-wing value. Of the remaining cases in this category, several were previously mentioned as being of doubtful value because of probable dimensional uncertainties or unrealistic aerodynamic assumptions.

CONCLUDING REMARKS

In the light of the foregoing discussion, it seems reasonable to conclude that this method of estimation, which has been developed by making use of certain broad assumptions, is capable of providing estimates of the changes in aileron rolling effectiveness for a wide range of wing-aileron configurations within the experimental accuracy of the rocket-model technique for changes up to 80 percent of the estimated rigid-wing values. The direct application of the results of this investigation to wing-aileron configurations wherein the aerodynamic and structural characteristics differ markedly from those assumed should be avoided. It is recommended that in these cases a closer approximation to the actual characteristics be used and a particular solution be obtained.

Langley Aeronautical Laboratory,
National Advisory Committee for Aeronautics,
Langley Field, Va., August 20, 1953.
(Corrected April 21, 1954.)

APPENDIX A

TYPICAL COMPUTING PROCEDURE USED IN THE ESTIMATION OF THE EFFECTS
OF AEROELASTICITY UPON THE STEADY-STATE ROLLING EFFECTIVENESS

The change in rolling effectiveness due to aeroelasticity for a wing wherein the structural parameters closely approximate those for a wing of homogeneous construction is given in equation (49). There are two ways in which the equation can be used.

(1) Estimation of rigid-wing values based upon measured flight data. Flight-test data are substituted into the equation and the effect of aeroelasticity is obtained directly.

(2) Estimation of flexible-wing values based upon rigid-wing values. It is very important that accurate values of $\left(\frac{pb/2V}{\delta}\right)_r$ be used.

In the following example both methods of estimation are demonstrated. Case 33 is fairly representative of the computing procedures used throughout this paper. This case is interesting because the construction of the test wings is such that the spanwise variations of GJ and EI of a full-scale fighter type of airplane are very closely approximated in the test wings, and for this reason, the measured effect of aeroelasticity should be very similar to that encountered by the actual airplane. A sketch of the wing-control configuration of the example case is presented as figure 20. In order to obtain the desired elastic characteristics, it was necessary to slot the outboard portion of the chord-plane aluminum-alloy stiffener and to orient the grain of the wood approximately 45° with respect to the 38-percent-chord line. Grain orientation permits alteration of the bending stiffness without appreciably affecting the torsional stiffness (ref. 4). A special test panel was built and tested with the wood grain at an angle of 45° with respect to the flexural axis. The results of this test in conjunction with the data from reference 4 are presented in figure 21. The flexural axes of all the wings tested were assumed to be at the 45-percent-chord line. The resulting angle between the grain direction and the assumed flexural axis was approximately 43.8° . The data from figure 21 show that the wood (spruce) was only 22 percent as stiff in bending as it would have been had the grain run parallel to the flexural axis. The material constants used in the calculations were:

For spruce

$$E = 1.4 \times 10^6 \text{ lb/sq in.} \times 0.22 = 0.31 \times 10^6 \text{ lb/sq in.}$$

$$G = 0.09 \times 10^6 \text{ lb/sq in.}$$

For 24S-T aluminum alloy

$$E = 10.8 \times 10^6 \text{ lb/sq in.}$$

$$G = 3.91 \times 10^6 \text{ lb/sq in.}$$

Modifying equation (12) gives:

$$\alpha_T = \int_0^x \frac{\left(1 + \tan^2 \Lambda_e \frac{GJ}{EI}\right)}{GJ} dx - \int_0^{\Delta x} \frac{\left(1 + \tan^2 \Lambda_e \frac{GJ}{EI}\right)}{GJ} dx$$

where at any given spanwise station x the following relationships are assumed:

$$GJ(\text{composite section}) \approx (GJ)_{(\text{alum. stiff.})} + (GJ)_{(\text{wood})}$$

$$EI(\text{composite section}) \approx (EI)_{(\text{alum. stiff.})} + (EI)_{(\text{wood})}$$

For simplification the identifying subscripts can be expressed as

A aluminum stiffener

W wood

Then

$$I_A = \frac{c_A t_A^3}{12}$$

where

c_A chord of stiffener parallel to model center line, in.

t_A thickness of stiffener parallel to model center line, in.

$$J_A \approx 4I_A$$

$$I_W \approx K_1 c t^3 - I_A \approx 0.0377 c t^3 - I_A$$

$$J_W \approx 4I_W$$

Δx spanwise distance of effective root from fuselage, in.

In figure 22 is illustrated a comparison of the experimental variation of α/T with exposed span with the calculated variation for three different locations of the effective root. The calculated values for $\Delta x = 0$ overestimate the twist considerably, particularly near the wing root. The agreement is considerably improved by the use of the effective root location from equation (29) ($\Delta x = 2.7$). As mentioned previously the method of attachment of the wings to the fuselage may permit appreciable movement of the wing root. Because of this fact, the effective root location which gave the best agreement with the experimental data was the one upon which the calculations were based ($\Delta x = 1.9$). The overall agreement is excellent between the experimental data and the calculated values when based upon the root located at $\Delta x = 1.9$.

The foregoing description illustrates the general procedure followed in all of the cases presented. This procedure was necessitated because of the extreme difficulty involved in the procurement of the desired structural values experimentally. The variation of α/T with span as presented is relatively easy to obtain and serves as an experimental check upon the validity of the structural assumptions. The values of the structural constants thus calculated at the midpoint of the exposed span were used in the estimation of the effects of aeroelasticity.

The test wings of case 33 were not homogeneous but, with the exception of the extreme tip region ($k > 0.92$), the variation of GJ/EI and c^4/GJ from a mean value was less than ± 10 percent across the span and suited for use in equation (49).

[REDACTED]

[REDACTED]

$$1 - \varphi = \frac{-q C_{L\alpha}^2 AR^2}{8 C_{L\delta}} \frac{c^4}{GJ} \left\{ \left(1 + \tan^2 \Lambda_e \frac{GJ}{EI} \right) \left(d_2 \alpha_6 \int_{k_R}^1 A \frac{c}{c} k dk - \right. \right. \\ \left. d_1 \frac{pb}{2V} \int_{k_R}^1 B \frac{c}{c} k dk \right) - \frac{AR}{2} \frac{GJ}{EI} \frac{\sin \Lambda_e}{\cos^3 \Lambda_e} \left(\alpha_6 \int_{k_R}^1 C \frac{c}{c} k dk - \right. \\ \left. \frac{pb}{2V} \int_{k_R}^1 D \frac{c}{c} k dk \right) \left. - \int_{k_R + \frac{\Delta k}{2}}^1 \frac{c}{c} k dk \left[\left(1 + \tan^2 \Lambda_e \frac{GJ}{EI} \right) \left(d_2 \alpha_6 \Delta A - \right. \right. \right. \right. \\ \left. \left. d_1 \frac{pb}{2V} \Delta B \right) - \frac{AR}{2} \frac{GJ}{EI} \frac{\sin \Lambda_e}{\cos^3 \Lambda_e} \left(\alpha_6 \Delta C - \frac{pb}{2V} \Delta D \right) \right] \right\}$$

where at $M = 0.8$

$$q = \frac{547}{144} = 3.80 \frac{\text{lb}}{\text{in}^2} \text{ (from flight data)}$$

$C_{L\alpha}$, α_6 , d_1 , d_2 are given in table III

$$AR = 3.4$$

$$\Lambda_e = 43.8^\circ$$

$$\Delta k = \frac{1.9 \text{ in.}}{13.148 \text{ in.}} = 0.145 \text{ (fig. 22)}$$

$$\frac{C_{L\delta}}{\alpha_6 C_{L\alpha}} = 0.115 \text{ (fig. 10)}$$

$$\lambda = 0.44$$

$$k_1 = 0.62$$

$$k_0 = 1.0$$

$$k_R = 0.19$$

$$\left. \begin{array}{l} \frac{GJ}{EI} = 1.30 \\ \frac{c^4}{GJ} = 0.0874 \end{array} \right\} \text{calculated}$$

$$\int_{k_R}^1 A \frac{c}{c} k dk = 0.0375 \text{ (fig. 4)}$$

$$\int_{k_R}^1 B \frac{c}{c} k dk = 0.0402 \text{ (fig. 6)}$$

$$\int_{k_R}^1 C \frac{c}{c} k dk = 0.0140 \text{ (fig. 8)}$$

$$\int_{k_R}^1 D \frac{c}{c} k dk = 0.0130 \text{ (fig. 6)}$$

$$\int_{k_R + \frac{\Delta k}{2}}^1 \frac{c}{c} k dk = 0.387 \text{ (fig. 3)}$$

Values obtained by cross plotting

$$\frac{\Delta A}{\Delta k} = 0.102 \text{ (fig. 5)}$$

$$\frac{\Delta B}{\Delta k} = 0.161 \text{ (fig. 7)}$$

$$\frac{\Delta C}{\Delta k} = 0.078 \text{ (fig. 9)}$$

$$\frac{\Delta D}{\Delta k} = 0.080 \text{ (fig. 7)}$$

Values obtained by cross plotting

$$\Delta A = \Delta k \frac{\Delta A}{\Delta k} = (0.145)(0.102) = 0.0148$$

$$\Delta B = \Delta k \frac{\Delta B}{\Delta k} = (0.145)(0.161) = 0.0233$$

$$\Delta C = \Delta k \frac{\Delta C}{\Delta k} = (0.145)(0.078) = 0.0113$$

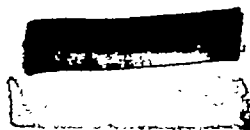
$$\Delta D = \Delta k \frac{\Delta D}{\Delta k} = (0.145)(0.080) = 0.0116$$

$$\begin{aligned} \int_{\Delta k}^1 A \frac{c}{c} k \, dk &= \int_{k_R}^1 A \frac{c}{c} k \, dk - \Delta A \int_{k_R + \frac{\Delta k}{2}}^1 \frac{c}{c} k \, dk \\ &= 0.0375 - (0.0148)(0.387) = 0.318 \end{aligned}$$

$$\begin{aligned} \int_{\Delta k}^1 B \frac{c}{c} k \, dk &= \int_{k_R}^1 B \frac{c}{c} k \, dk - \Delta B \int_{k_R + \frac{\Delta k}{2}}^1 \frac{c}{c} k \, dk \\ &= 0.0402 - (0.0233)(0.387) = 0.0312 \end{aligned}$$

$$\begin{aligned} \int_{\Delta k}^1 C \frac{c}{c} k \, dk &= \int_{k_R}^1 C \frac{c}{c} k \, dk - \Delta C \int_{k_R + \frac{\Delta k}{2}}^1 \frac{c}{c} k \, dk \\ &= 0.0140 - (0.0113)(0.387) = 0.0096 \end{aligned}$$

$$\begin{aligned} \int_{\Delta k}^1 D \frac{c}{c} k \, dk &= \int_{k_R}^1 D \frac{c}{c} k \, dk - \Delta D \int_{k_R + \frac{\Delta k}{2}}^1 \frac{c}{c} k \, dk \\ &= 0.0130 - (0.0116)(0.387) = 0.0085 \end{aligned}$$



Substituting into equation (49) gives at $M = 0.8$, for example

$$1 - \phi = -(3.80)(102.1)(0.0874) \left\{ 2.20 \left[-0.00025 - 0.00624 \left(\frac{pb/2V}{\delta} \right)_f \right] - \right. \\ \left. 4.07 \left[0.00374 - 0.0085 \left(\frac{pb/2V}{\delta} \right)_f \right] \right\} = -33.91 \left[-0.015772 + 0.020867 \left(\frac{pb/2V}{\delta} \right)_f \right] \quad (A1)$$

Method 1. - Estimation of effect of aeroelasticity based upon flexible-wing data. From test of case 33

$$\left(\frac{pb/2V}{\delta} \right)_f = 0.135 \quad \text{at } M = 0.8$$

then

$$1 - \phi = 0.439 \quad \text{or} \quad \phi = 0.561$$

If it is necessary to estimate the loss in rolling effectiveness and rigid-wing values are available, the procedure advocated is as follows:

Method 2. - From estimated rigid-wing values based upon case 32 at $M = 0.8$, $\left(\frac{pb}{2V} \right)_r = 0.051$ ($\delta_\alpha = 10^\circ$ normal to hinge axis); sweep of aileron hinge axis $\approx 38.8^\circ$; δ_α (parallel to model center line) = $10^\circ \cos 38.8^\circ = 10^\circ \times 0.77 = 7.7^\circ$

$$\left(\frac{pb/2V}{\delta} \right)_r = \frac{0.051}{7.7} = 0.00663 \text{ radian/deg} = 0.379 \text{ rad/rad}$$

$$\left(\frac{pb/2V}{\delta}\right)_f = \left(\frac{pb/2V}{\delta}\right)_r \phi \quad (A2)$$

Substituting for $\left(\frac{pb/2V}{\delta}\right)_f$ into equation (A1) gives

$$1 - \phi = -33.91 \left[-0.015772 + (0.020867)(0.379)\phi \right] \quad (A3)$$

Solution of this equation gives $\phi = 0.636$.

The difference between the values for ϕ obtained by the two methods is well within the estimated experimental error of the data.

APPENDIX B

COMPARISON OF SOME EXPERIMENTALLY DETERMINED STRUCTURAL CONSTANTS
WITH THOSE CALCULATED BY APPROXIMATE METHODS

During the course of this investigation, it was found necessary to construct several special test panels in order to obtain structural data for design purposes. These were supplemented with a few additional test panels primarily designed to indicate the limits of applicability of the approximate formulas used in determining the structural constants c^4/GJ and GJ/EI for use in the aeroelastic calculations. The results of these tests in conjunction with the calculated values are presented in table IV in the hope that they may prove useful to other investigators operating under similar circumstances.

The experimental values were obtained in the following manner:

EI.- The test panels were simply supported at the ends and a concentrated load P applied at the center. EI was obtained from the relationship

$$EI = \frac{Pl^3}{48\delta}$$

where

- P applied load, lbs
 l distance between supports, 28 in.
 δ maximum deflection of test panel, in.

The load P was applied on, and the deflection δ was measured at the flexural axis of the beam which was obtained by special tests (approximately $0.45c \pm 0.10c$).

GJ.- The test panels were rigidly clamped at one end and a torque T was applied at the other end. GJ was obtained from the relationship

$$GJ = \frac{Tl}{\theta}$$

where

T applied torque, in-lb

θ angle of twist, radians

l distance between root and point of twist measurement, 28 in.

The calculated values were obtained in a manner similar to that illustrated in appendix A. In addition, most of the test panels employed metal inlays set into the surface of the wood. The stiffening effect of these inlays in both bending and torsion was determined assuming that the curved inlays could be considered as flat plates whose distance from the chord plane was equal to the mean effective distance of the curved inlays from the chord plane where

$$\text{Mean effective distance} = \left(\frac{\int_0^x y^3 dx}{x} \right)^{1/3}$$

EI.-

$$EI(\text{composite}) = EI(\text{stiffener}) + EI(\text{corestock}) + EI(\text{inlays})$$

where

$$I(\text{inlays}) = \frac{c_1(d_1^3 - d_2^3)}{12}$$

where

c_1 chord of inlay, in.

d_1 twice mean effective distance of outer surface of inlay from chord plane

d_2 twice mean effective distance of inner surface of inlay from chord plane

CONFIDENTIAL

$$I_{(\text{corestock})} = 0.0377ct^3 - I_{(\text{stiffener})} - I_{(\text{inlay})}$$

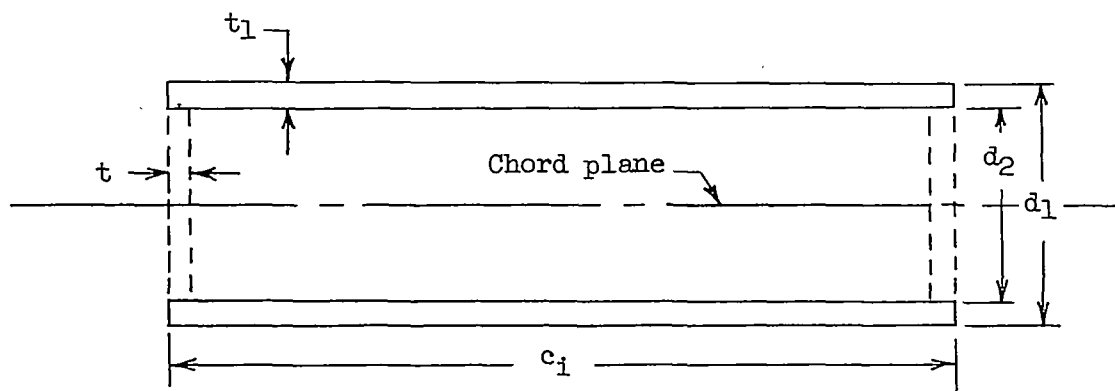
GJ.-

$$GJ_{(\text{composite})} = GJ_{(\text{stiffener})} + GJ_{(\text{corestock})} + GJ_{(\text{inlay})}$$

where $J_{(\text{inlays})}$ is computed assuming that the inlays make up two of the opposing sides of a hollow rectangular section. (This equation is from ref. 2 with the symbols altered to conform to those used in the present paper.)

$$J = \frac{2tt_1(c_1 - t)^2(d_1 - t_1)^2}{c_1t + d_1t_1 - t^2 - t_1^2}$$

where



$t = t_1 = \text{thickness of inlay, inches}$

CONFIDENTIAL

REFERENCES

1. Zender, George W., and Brooks, William A., Jr.: An Approximate Method of Calculating the Deformations of Wings Having Swept, M or W, A, and Swept-Tip Plan Forms. NACA TN 2978, 1953.
2. Roark, Raymond J.: Formulas for Stress and Strain. Second ed., McGraw-Hill Book Co., Inc., 1943.
3. Strass, H. Kurt, and Marley, Edward T.: Rolling Effectiveness of All-Movable Wings at Small Angles of Incidence at Mach Numbers From 0.6 to 1.6. NACA RM L51H03, 1951.
4. Anon.: Design of Wood Aircraft Structures. ANC Bulletin-18, Army-Navy-Civil Committee on Aircraft Design Criteria, June 1944.
5. Strass, H. Kurt, Fields, E. M., and Purser, Paul E.: Experimental Determination of Effect of Structural Rigidity on Rolling Effectiveness of Some Straight and Swept Wings at Mach Numbers From 0.7 to 1.7. NACA RM L50G14b, 1950.
6. Schult, Eugene D., Strass, H. Kurt, and Fields, E. M.: Free-Flight Measurements of Some Effects of Aileron Span, Chord, and Deflection and of Wing Flexibility on the Rolling Effectiveness of Ailerons on Sweptback Wings at Mach Numbers Between 0.8 and 1.6. NACA RM L51K16, 1952.
7. Strass, H. Kurt, and Marley, Edward T.: Rocket-Model Investigation of the Rolling Effectiveness of a Fighter-Type Wing-Control Configuration at Mach Numbers From 0.6 to 1.5. NACA RM L51I28, 1951.
8. Strass, H. Kurt, Fields, E. M., and Schult, Eugene D.: Some Effects of Spanwise Aileron Location and Wing Structural Rigidity on the Rolling Effectiveness of 0.3-Chord Flap-Type Ailerons on a Tapered Wing Having 63° Sweepback at the Leading Edge and NACA 64A005 Airfoil Sections. NACA RM L51D18a, 1951.

TABLE I.- GEOMETRIC CHARACTERISTICS OF TEST WINGS

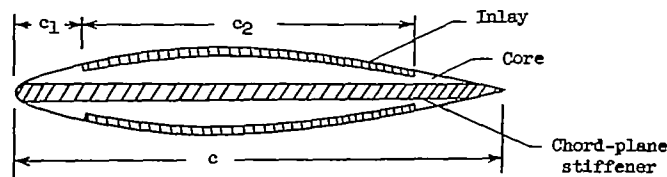
Case	$\Lambda_c/4$, deg	A	λ	k_1	k_0	c_a/c	NACA airfoil section	Reference
1,2	0	3.7	1.00	0.19	1.0	0.2	65A003	5
3-8	0	3.7	1.00	.19	1.0	.2	65A009	5
9-13	45	3.7	1.00	.19	1.0	.2	65A009	5
14,15	45	8.0	1.00	.13	1.0	.2	65 ₁ A012	Unreported
16,17	45	8.0	.50	.13	1.0	.2	65 ₁ A012	Unreported
18-20	45	4.0	.60	.14	1.0	.3	65A006	^a 6
21-23	45	4.0	.60	.57	1.0	.3	65A006	6
24,25	45	4.0	.60	.14	.57	.3	65A006	6
26,27	35	4.0	.60	.14	1.0	.3	65A006	6
28,29	45	3.0	.50	.68	1.0	.25	000X-1.16 38/1.14 (modified); 9 percent at root, 7 percent at tip	7
30,31	20	5.9	.47	.70	1.0	.2	64-OXX normal to 38 percent c; 11 percent at root, 8.28 percent at tip	Unreported
32,33	48	3.4	.44	.62	1.0	.2	64-OXX normal to 38 percent c; 11 percent at root, 8.28 percent at tip	Unreported
34-36	61	3.5	.25	.50	1.0	.3	64A005	8

^aCase 19 previously not reported.

NACA

TABLE II.- CONSTRUCTIONAL CHARACTERISTICS OF TEST WINGS

[Typical section through wing at mid-span. All dimensions are in inches]



Case	Material of Construction			c	c ₁ /c	c ₂ /c	c ⁴ /GJ	GJ/EI	Number of nominally identical models
	Inlay	Core	Stiffener						
1	None	Steel	None	7.07	----	----	0.0184	1.43	1
2	None	Aluminum alloy	None	7.07	----	----	.0556	1.45	1
3	0.02 steel	Spruce	None	7.07	0.1	0.8	.0067	1.04	3
4	0.016 aluminum alloy	Spruce	None	7.07	.1	.8	.0158	.59	1
5	None	White pine	None	7.07	----	----	.0579	.25	1
6	0.01 steel	Spruce	None	7.07	.1	.8	.0100	.84	2
7	None	Beech	None	7.07	----	----	.0371	.25	2
8	None	White pine	None	7.07	----	----	.0603	.25	1
9	0.02 steel	Spruce	None	7.07	.1	.8	.0067	1.04	2
10	None	Beech	None	7.07	----	----	.0377	.25	1
11	0.01 steel	Spruce	None	7.07	.1	.8	.0095	.84	1
12	0.016 aluminum alloy	Spruce	None	7.07	.1	.8	.0161	.59	2
13	None	White pine	None	7.07	----	----	.0750	.25	2
14	None	Aluminum alloy	None	4.66	----	----	.0010	1.45	1
15	0.010 steel	Spruce	0.063 aluminum alloy	4.66	.1	.8	.0030	.85	1
16	None	Steel	None	4.66	----	----	.0004	1.43	1
17	0.010 steel	Spruce	0.063 aluminum alloy	4.66	.1	.8	.0030	.85	1
18	0.040 steel	Spruce	0.125 aluminum alloy	8.99	.15	.7	.0080	.98	1
19	None	Aluminum alloy	None	8.99	----	----	.0079	1.45	1
20	None	Beech	0.125 aluminum alloy	8.99	----	----	.1070	.47	1
21	0.040 steel	Spruce	0.125 aluminum alloy	8.99	.15	.7	.0080	.98	1
22	None	Aluminum alloy	None	8.99	----	----	.0079	1.45	1
23	None	Mahogany	0.125 aluminum alloy	8.99	----	----	.1290	.46	1
24	0.040 steel	Spruce	0.125 aluminum alloy	8.99	.15	.7	.0080	.98	1
25	None	Beech	0.125 aluminum alloy	8.99	----	----	.1070	.47	1
26	None	Aluminum alloy	None	8.99	----	----	.0079	1.45	1
27	None	Mahogany	0.125 aluminum alloy	8.99	----	----	.1290	.46	1
28	0.080 steel	Mahogany	0.125 aluminum alloy	11.37	a	a	.0039	.91	1
29	None	Mahogany	0.125 aluminum alloy ^b	11.37	----	----	.0931	.31	1
30	0.040 steel	Spruce	0.125 aluminum alloy	5.85	.1	.8	.0022	.97	1
31	None	Spruce	0.125 aluminum alloy ^b	5.85	----	----	.0423	1.29	1
32	0.040 steel	Spruce	0.125 aluminum alloy	7.77	.1	.8	.0047	1.00	1
33	None	Spruce	0.125 aluminum alloy ^c	7.77	----	----	.0874	1.30	1
34	None	Steel	None	7.69	----	----	.0053	1.43	1
35	None	Aluminum alloy	None	7.69	----	----	.0136	1.45	1
36	None	Beech	0.063 aluminum alloy	7.69	----	----	.2400	.39	1

^ac₁/c and c₂/c vary with span - see reference 6 for details.

^bChord-plane stiffener slotted - see reference 6 for details.

^cChord-plane stiffener slotted - see appendix A for details.

NACA

TABLE III.- ASSUMED AERODYNAMIC CHARACTERISTICS OF TEST WINGS

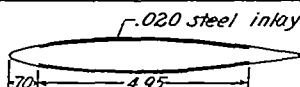
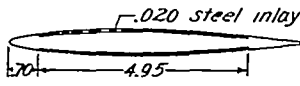
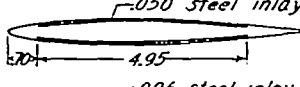
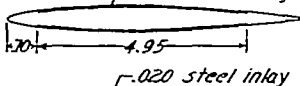
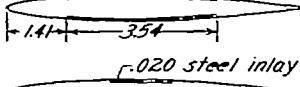
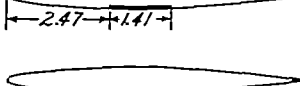

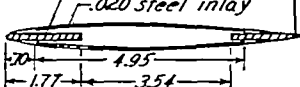
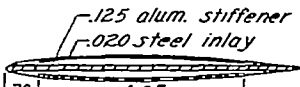
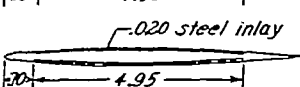
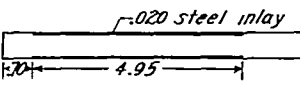
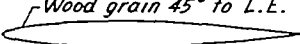
M	$C_{L\alpha}$	α_0	d_1	d_2
Cases 1 and 2				
0.6	3.98	0.49	0.20	-0.02
.7	4.47	.47	.20	-.02
.8	4.67	.43	.20	-.02
.9	4.80	.31	.10	-.18
1.0	4.40	.22	0	-.40
1.2	3.58	.16	0	-.40
1.4	3.07	.16	0	-.40
1.6	2.65	.16	0	-.40
Cases 3 to 8				
0.6	3.75	0.41	0.20	-0.02
.7	4.27	.38	.20	-.02
.8	4.50	.32	.20	-.02
.9	3.96	.27	.10	-.18
1.0	4.22	.17	0	-.40
1.2	3.48	.16	0	-.40
1.4	3.00	.16	0	-.40
1.6	2.64	.16	0	-.40
Cases 9 to 13				
0.6	---	---	---	---
.7	3.40	0.46	0.20	-0.02
.8	3.60	.44	.20	-.02
.9	3.80	.31	.10	-.18
1.0	3.40	.17	0	-.40
1.2	2.90	.16	0	-.40
1.4	2.72	.16	0	-.40
1.6	2.68	.16	0	-.40
Cases 14 and 15				
0.6	3.53	0.37	0.20	-0.02
.7	3.70	.33	.20	-.02
.8	3.85	.32	.20	-.02
.9	3.90	.28	.10	-.18
1.0	3.50	.17	0	-.40
1.2	2.75	.16	0	-.40
1.4	2.16	.16	0	-.40
1.6	---	---	---	---
Cases 16 and 17				
0.6	3.53	0.37	0.20	-0.02
.7	3.70	.33	.20	-.02
.8	3.85	.32	.20	-.02
.9	3.90	.28	.10	-.18
1.0	3.50	.17	0	-.40
1.2	2.75	.16	0	-.40
1.4	2.16	.16	0	-.40
1.6	---	---	---	---

M	$C_{L\alpha}$	α_0	d_1	d_2
Cases 18 to 20				
0.6	---	---	---	---
.7	3.41	0.60	0.20	0.02
.8	3.58	.56	.20	.02
.9	3.84	.43	.10	-.14
1.0	3.44	.26	0	-.35
1.2	2.87	.24	0	-.35
1.4	2.75	.24	0	-.35
1.6	2.66	.24	0	-.35
Cases 21 to 23				
0.6	---	---	---	---
.7	3.41	0.60	0.20	0.02
.8	3.58	.56	.20	.02
.9	3.84	.43	.10	-.14
1.0	3.44	.26	0	-.35
1.2	2.87	.24	0	-.35
1.4	2.75	.24	0	-.35
1.6	2.66	.24	0	-.35
Cases 24 and 25				
0.6	---	---	---	---
.7	3.41	0.60	0.20	0.02
.8	3.58	.56	.20	.02
.9	3.84	.43	.10	-.14
1.0	3.44	.26	0	-.35
1.2	2.87	.24	0	-.35
1.4	2.75	.24	0	-.35
1.6	2.66	.24	0	-.35
Cases 26 and 27				
0.6	3.78	---	---	---
.7	3.96	0.60	0.20	0.02
.8	4.22	.56	.20	.02
.9	4.57	.43	.10	-.14
1.0	4.10	.26	0	-.35
1.2	3.19	.24	0	-.35
1.4	2.84	.24	0	-.35
1.6	2.70	.24	0	-.35

M	$C_{L\alpha}$	α_0	d_1	d_2
Cases 28 and 29				
0.6	---	---	---	---
.7	3.41	0.63	0.20	0
.8	3.58	.57	.20	0
.9	3.84	.53	.10	-.16
1.0	3.44	.27	0	-.38
1.2	2.87	.24	0	-.38
1.4	2.75	.24	0	-.38
1.6	2.66	.24	0	-.38
Cases 30 and 31				
0.6	3.35	0.33	0.20	-0.02
.7	3.63	.33	.20	-.02
.8	3.91	.32	.20	-.02
.9	4.18	.28	.10	-.18
1.0	3.74	.17	0	-.40
1.2	2.97	.13	0	-.40
1.4	2.73	.13	0	-.40
1.6	2.63	.13	0	-.40
Cases 32 and 33				
0.6	---	---	---	---
.7	3.04	0.43	0.20	-0.02
.8	3.17	.39	.20	-.02
.9	3.25	.30	.10	-.18
1.0	3.00	.20	0	-.40
1.2	2.59	.15	0	-.40
1.4	2.46	.15	0	-.40
1.6	2.46	.15	0	-.40
Cases 34 to 36				
0.6	---	---	---	---
.7	2.94	0.60	0.20	0.02
.8	3.15	.56	.20	.02
.9	3.41	.43	.10	-.14
1.0	3.28	.26	0	-.35
1.2	2.77	.22	0	-.35
1.4	2.50	.22	0	-.35
1.6	2.34	.22	0	-.35

NACA

TABLE IV
STRUCTURAL CONSTANTS FOR A VARIETY OF TYPES OF WING CONSTRUCTION

	Test panel	Airfoil section	Experimental			Calculated		
			$EI \times 10^3$	$GJ \times 10^3$	GJ/EI	$EI \times 10^3$	$GJ \times 10^3$	GJ/EI
1		65A012	839	882	1.05	919	885	0.96
2		65A009	425	488	1.15	456	473	1.04
3		65A009	709	810	1.15	854	1,003	1.18
4		65A009	207	176	.85	227	173	.76
5		65A009	376	324	.86	402	386	.96
6		65A009	233	90	.39	250	163	.65
7		65A009	103	39	.38	123	33	.27
8		65A009	423	496	1.17	461	483	1.05
9		65A009	474	557	1.27	466	491	1.05
10		65A006	156	190	1.22	166	189	1.14
11		.09 slab	639	625	.98	586	640	1.09
12		65A009	22	41	1.87	—	—	—

Note: Core is mahogany ; $c = 7.071$ inches ; all dimensions are in inches.

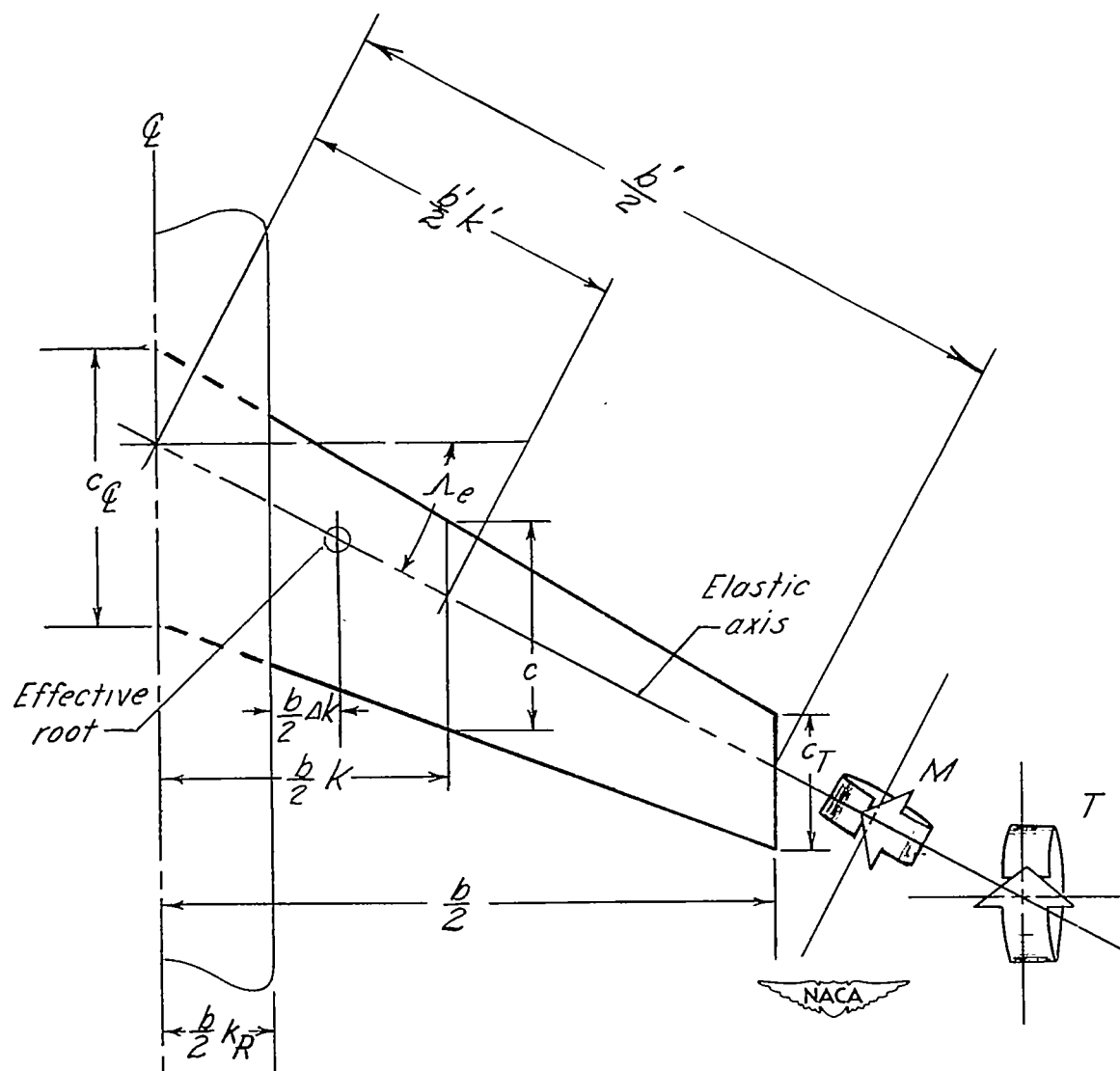


Figure 1.- The configuration considered in the structural analysis, showing planes of action of applied moments.

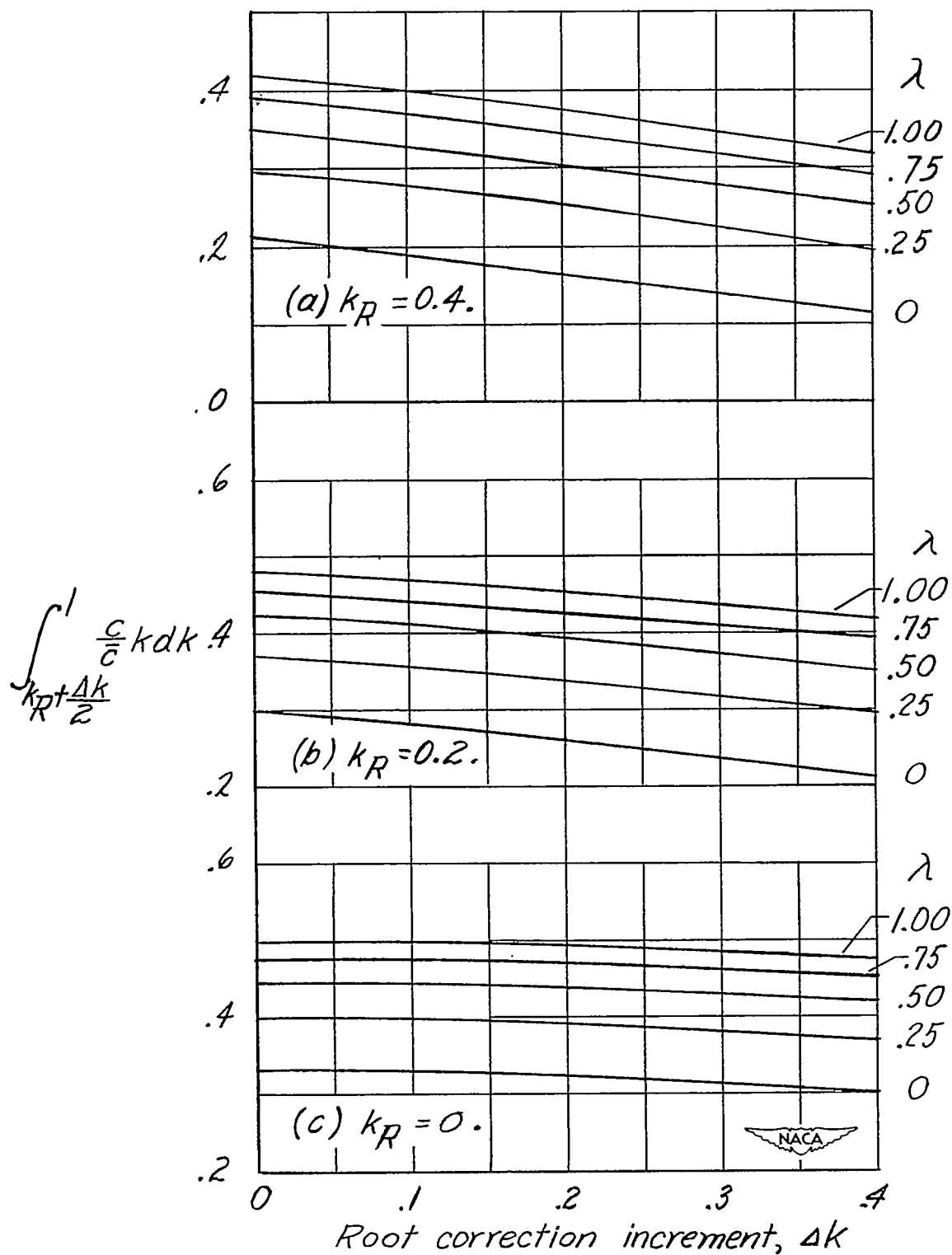


Figure 3.- Root correction factor for nondimensional rolling moments.

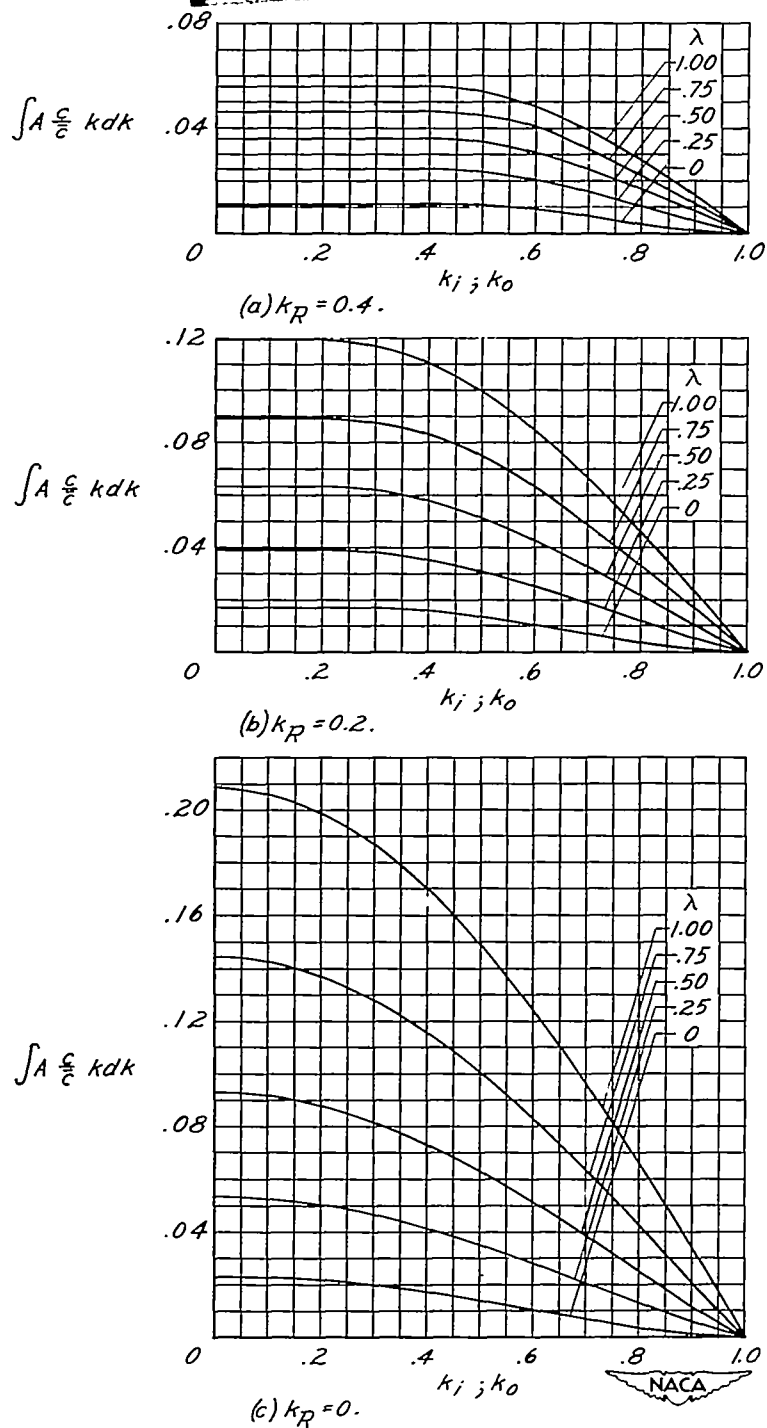
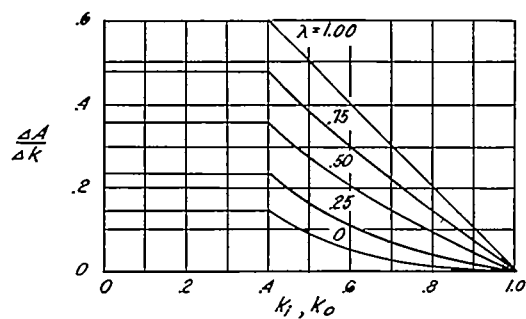
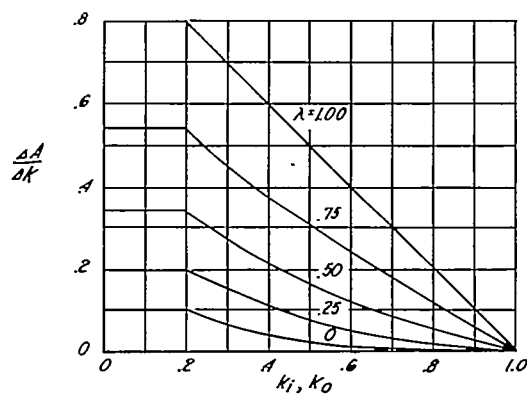
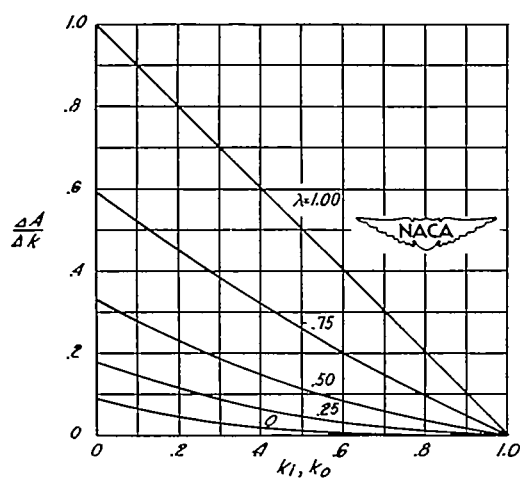


Figure 4.- Nondimensional rolling moments resulting from the deformations caused by the torques of the aileron loads about the elastic axis.

$$\int_{k_1}^{k_0} A \frac{c}{c} k dk = \int A \frac{c}{c} k dk \text{ at } k_1 - \int A \frac{c}{c} k dk \text{ at } k_0.$$

L

(a) $k_R = 0.4$.(b) $k_R = 0.2$.(c) $k_R = 0$.Figure 5.- Root correction factor for nondimensional angle of twist, A .

$$\left[\frac{\Delta A}{\Delta k} \right]_{k_1}^{k_0} = \frac{\Delta A}{\Delta k} \text{ at } k_1 - \frac{\Delta A}{\Delta k} \text{ at } k_0.$$

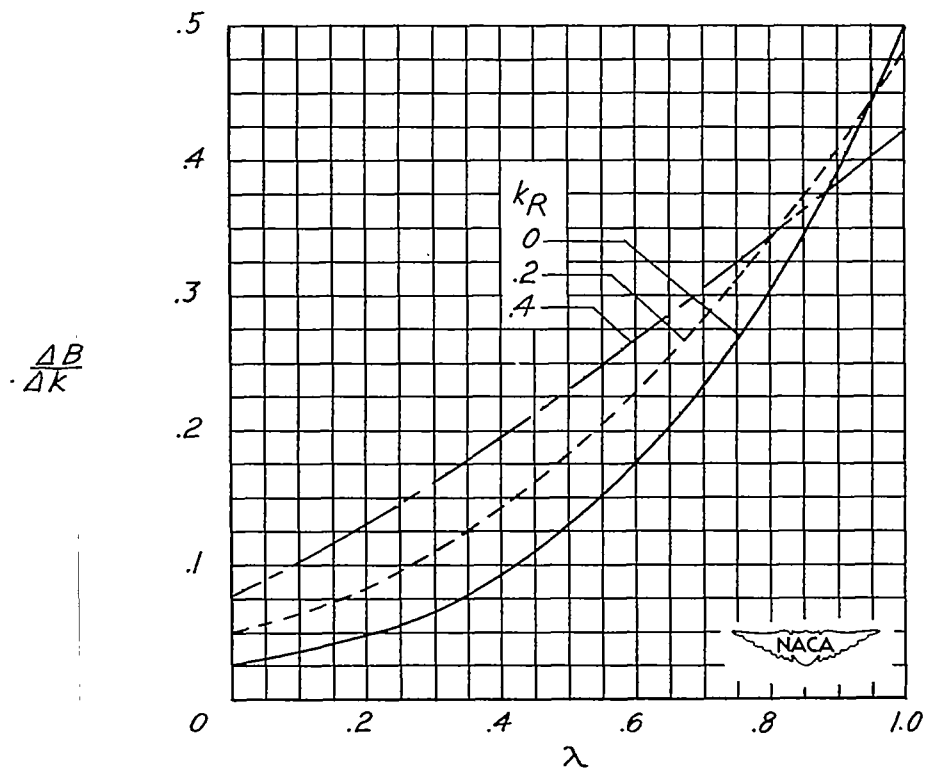
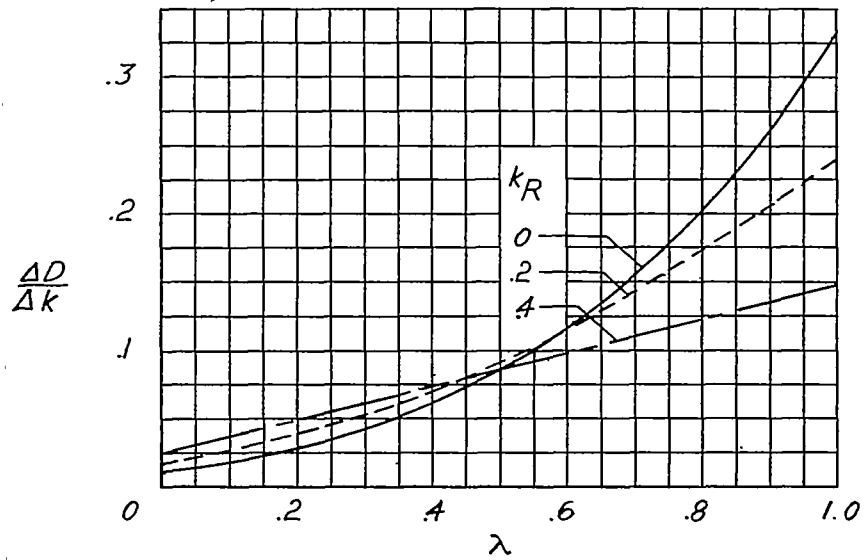


Figure 7.- Root correction factors for nondimensional angles of twist, B and D.

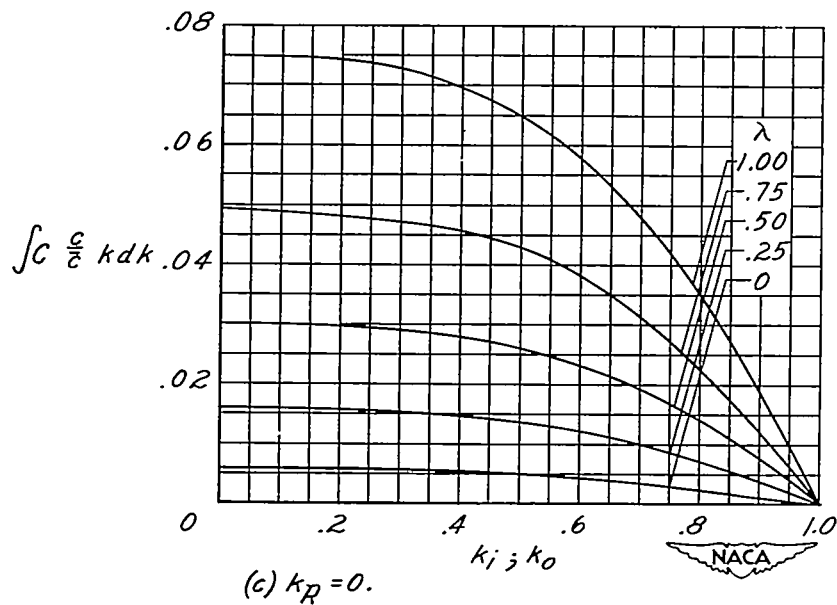
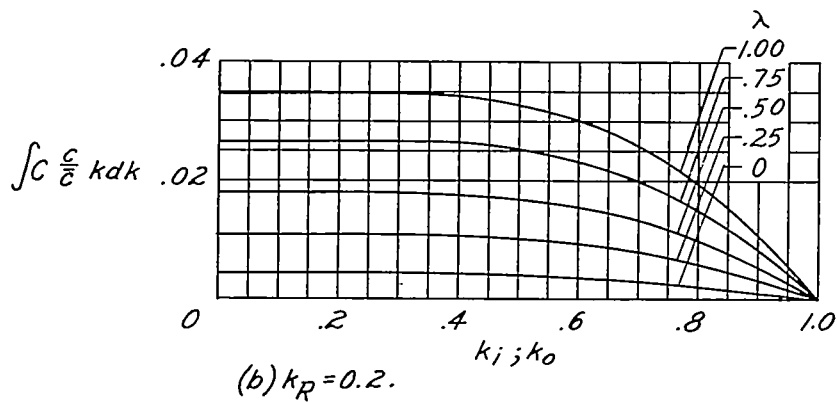
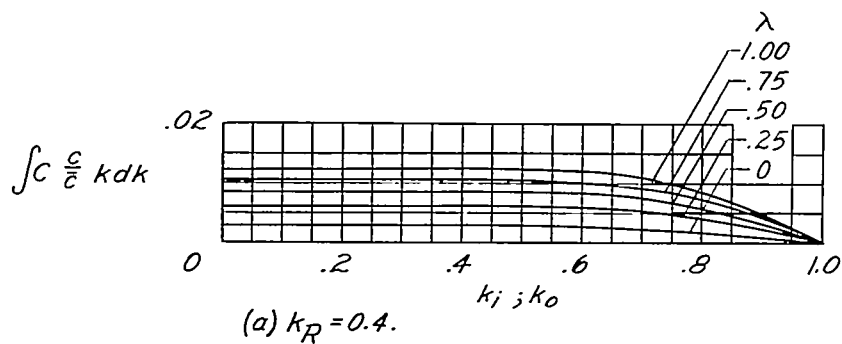
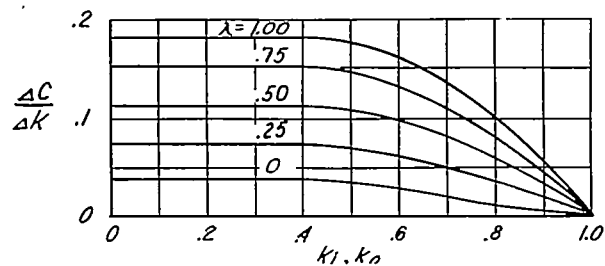
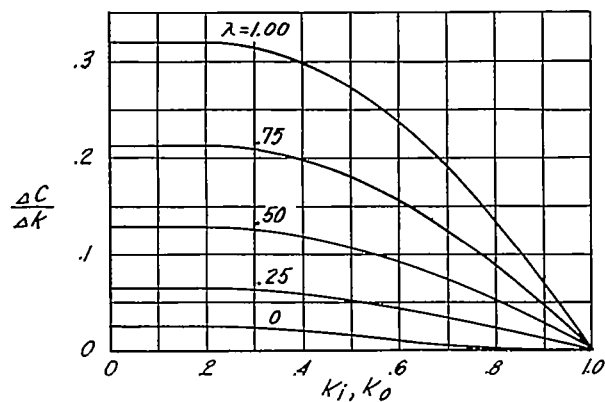


Figure 8.- Nondimensional rolling moments resulting from the deformations caused by the aileron loads on the elastic axis.

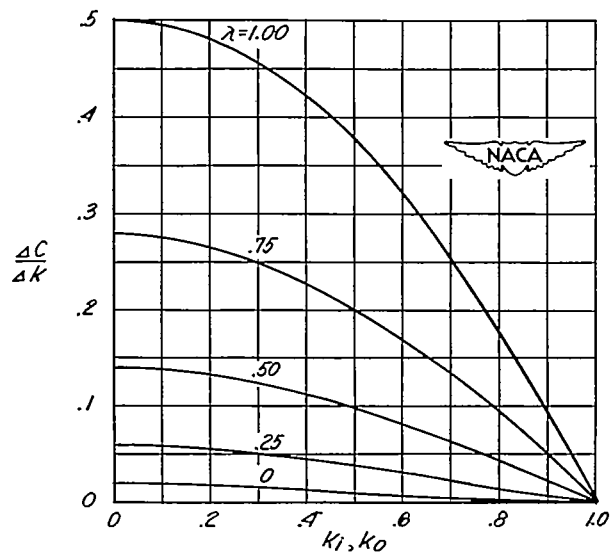
$$\int_{k_1}^{k_0} C \frac{c}{\bar{c}} k dk = \int C \frac{c}{\bar{c}} k dk \text{ at } k_1 - \int C \frac{c}{\bar{c}} k dk \text{ at } k_0.$$



(a) $k_R = 0.4$.



(b) $k_R = 0.2$.



(c) $k_R = 0$.

Figure 9.- Root correction factor for nondimensional angle of twist, C .

$$\left. \frac{\Delta C}{\Delta k} \right|_{k_i}^{k_o} = \frac{\Delta C}{\Delta k} \text{ at } k_i - \frac{\Delta C}{\Delta k} \text{ at } k_o.$$

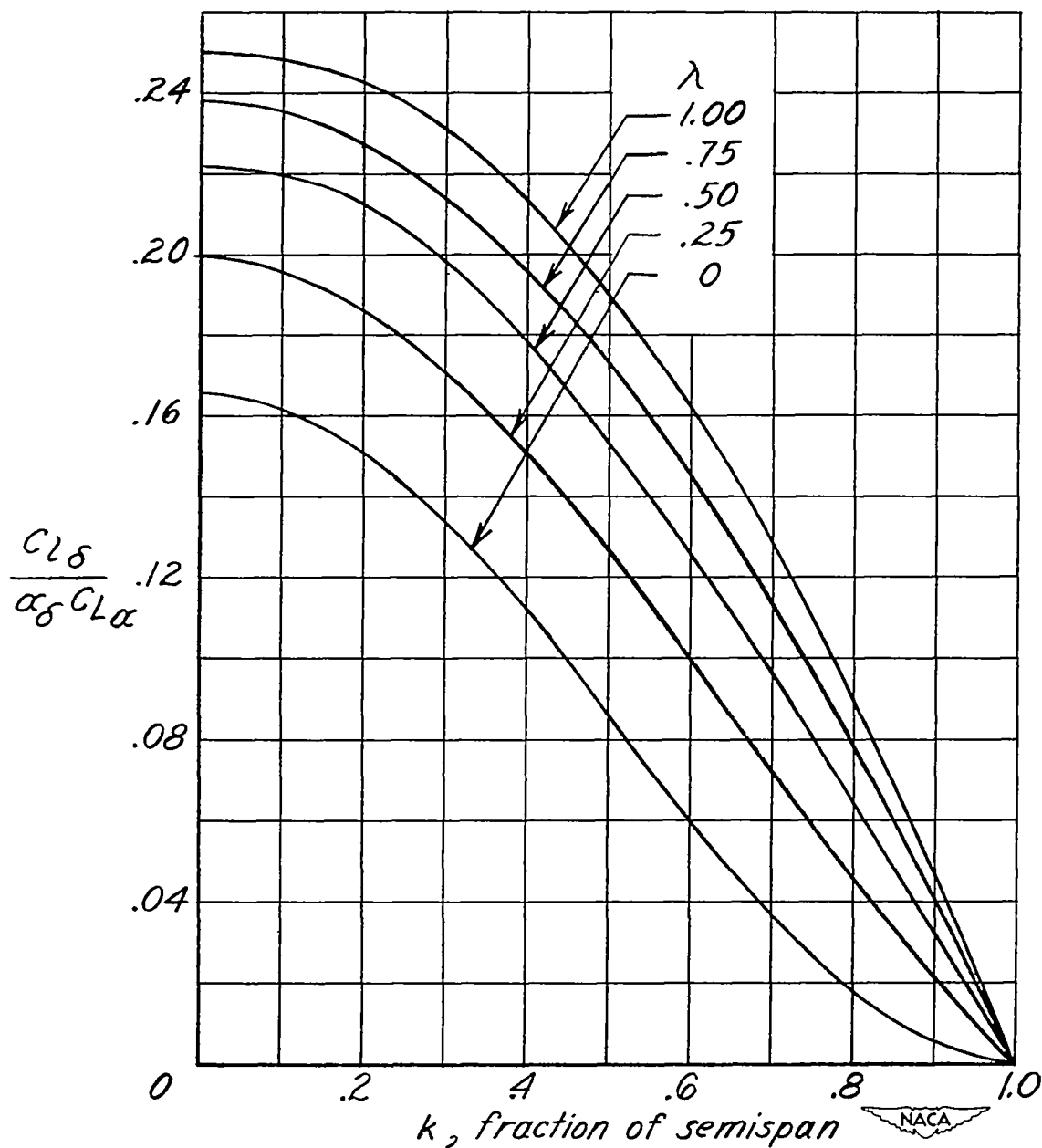
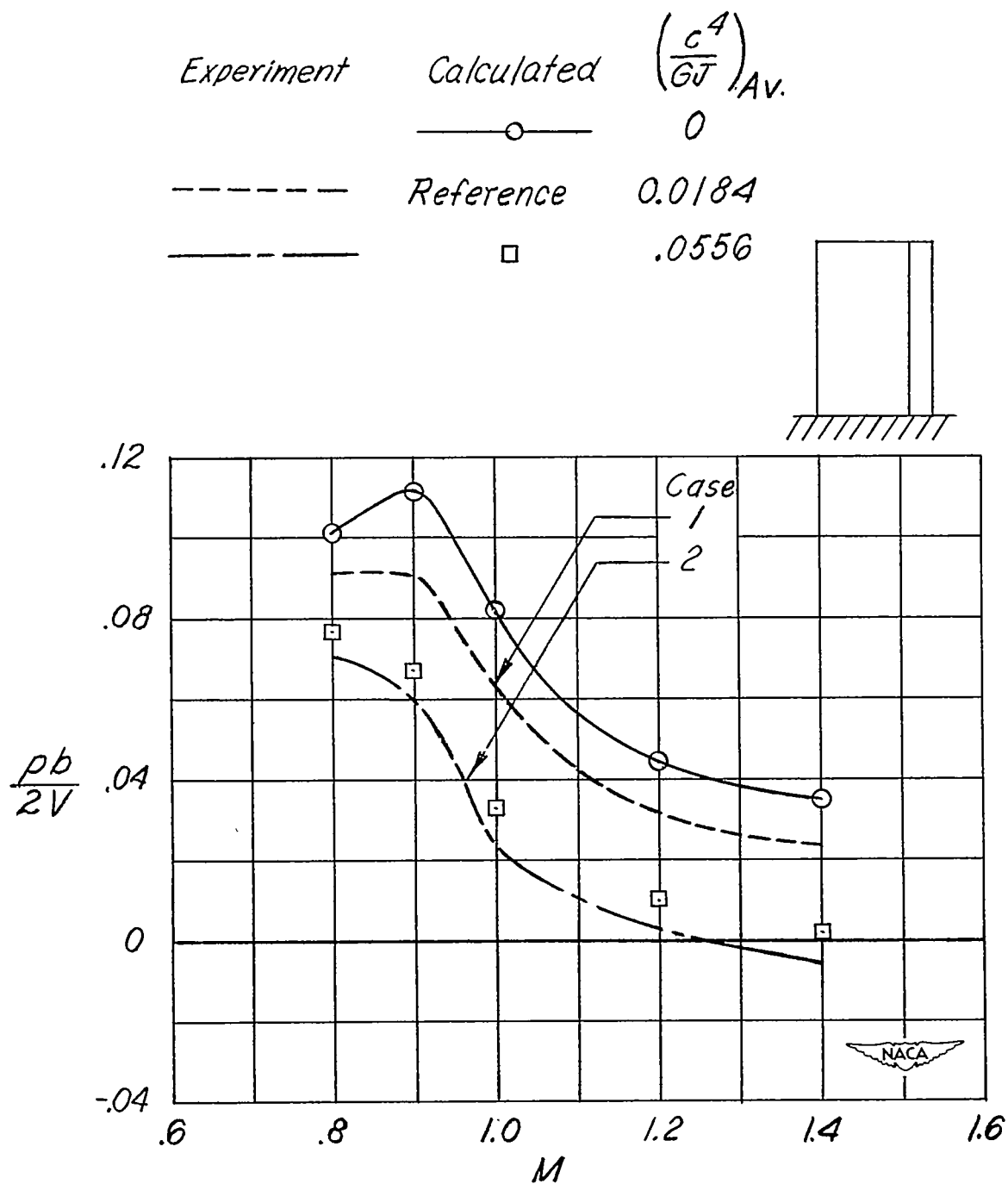


Figure 10.- Variation of nondimensional rolling moment with spanwise extent

and location of the aileron. $\left. \frac{C_{l\delta}}{\alpha_\delta C_{L\alpha}} \right|_{k_1}^{k_0} = \frac{C_{l\delta}}{\alpha_\delta C_{L\alpha}} \text{ at } k_1 - \frac{C_{l\delta}}{\alpha_\delta C_{L\alpha}} \text{ at } k_0.$



(a) NACA 65A003 airfoil section.

Figure 11.- Effect of decreasing wing stiffness on the variation of rolling effectiveness with Mach number. $AR = 3.7$; $\Lambda = 0^\circ$; $\lambda = 1.0$; $\delta_a = 5^\circ$; $k_1 = 0.19$; $k_0 = 1.0$.

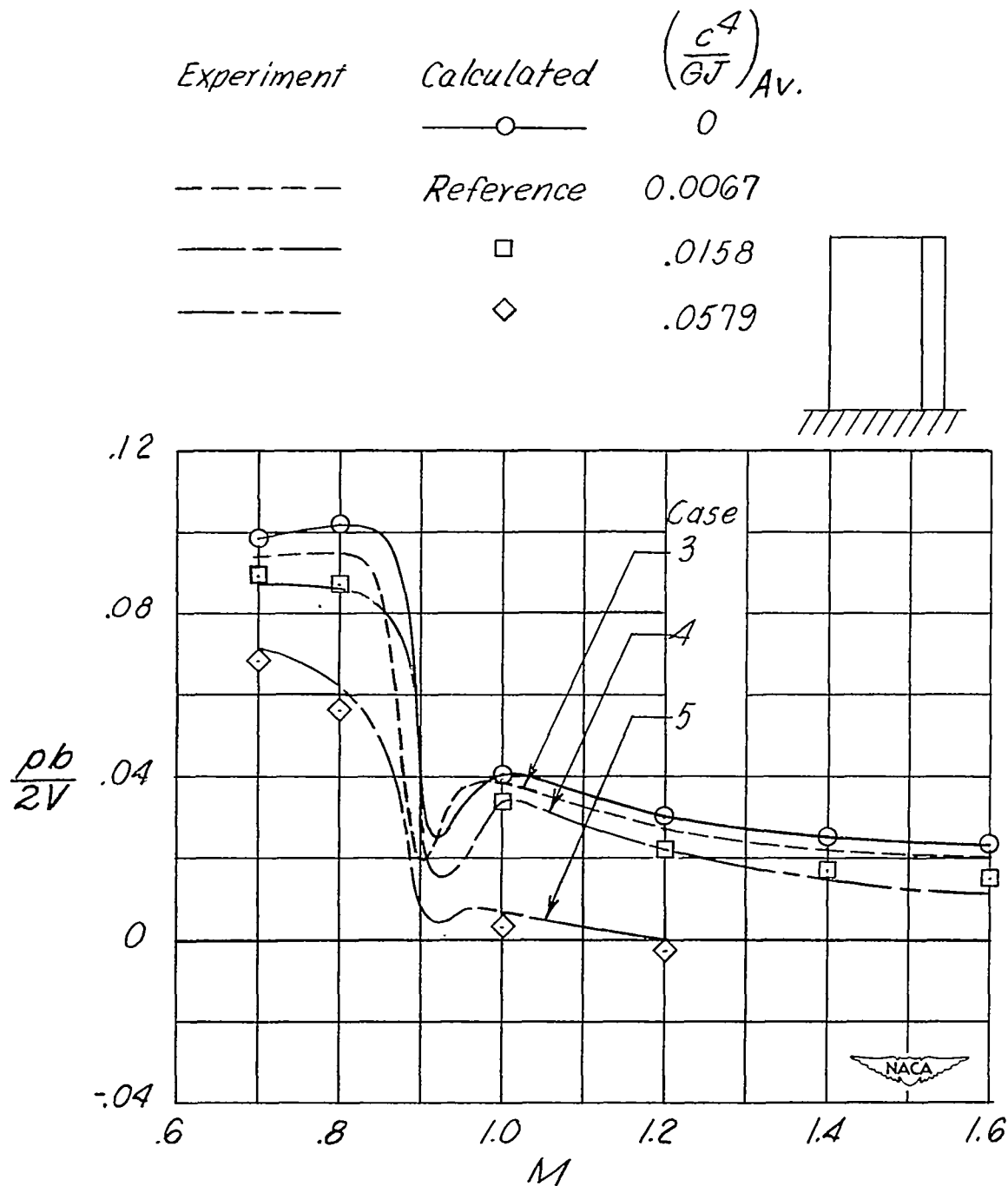
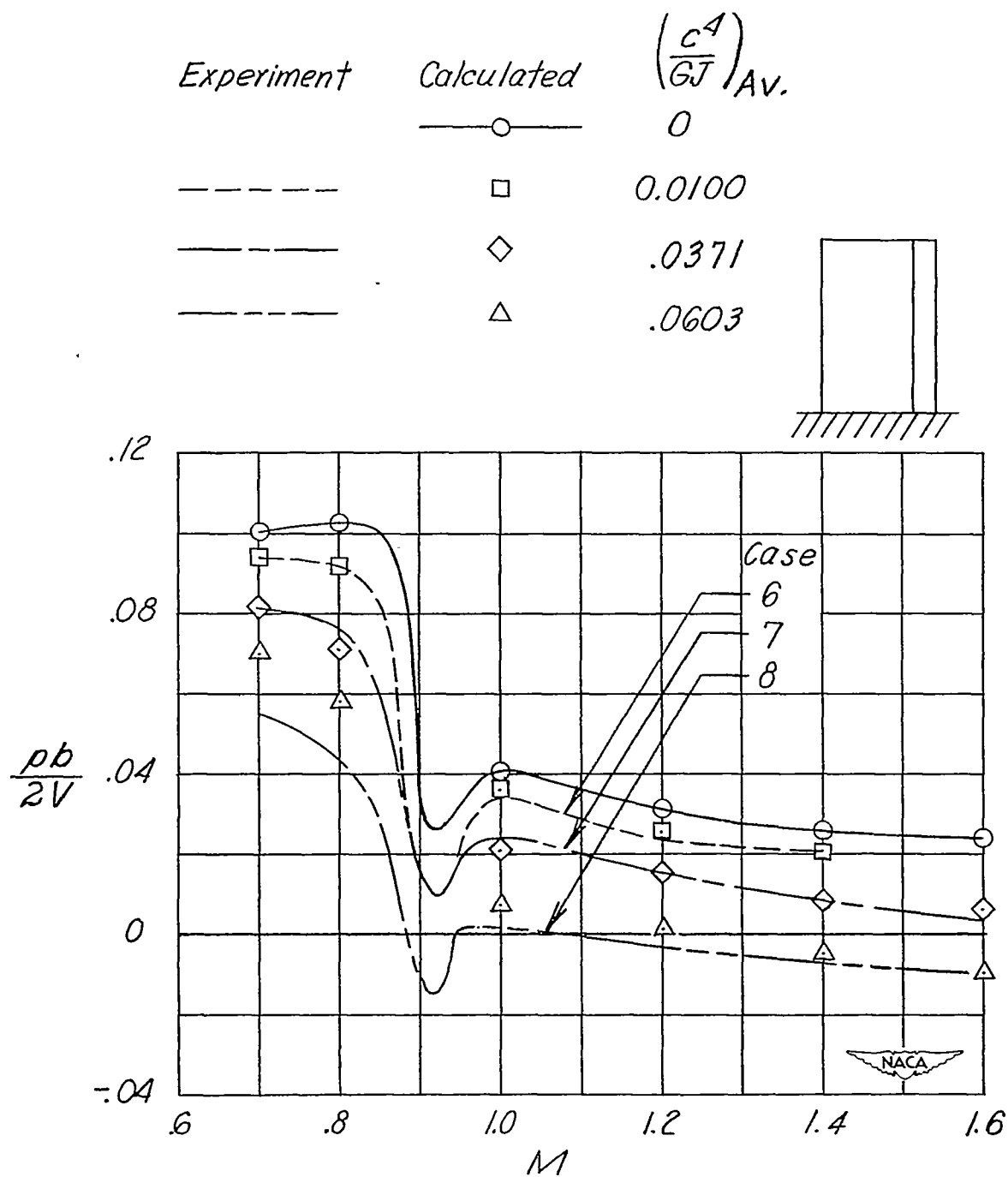


Figure 11.- Continued.



(b) Concluded.

Figure 11.- Concluded.

CONFIDENTIAL

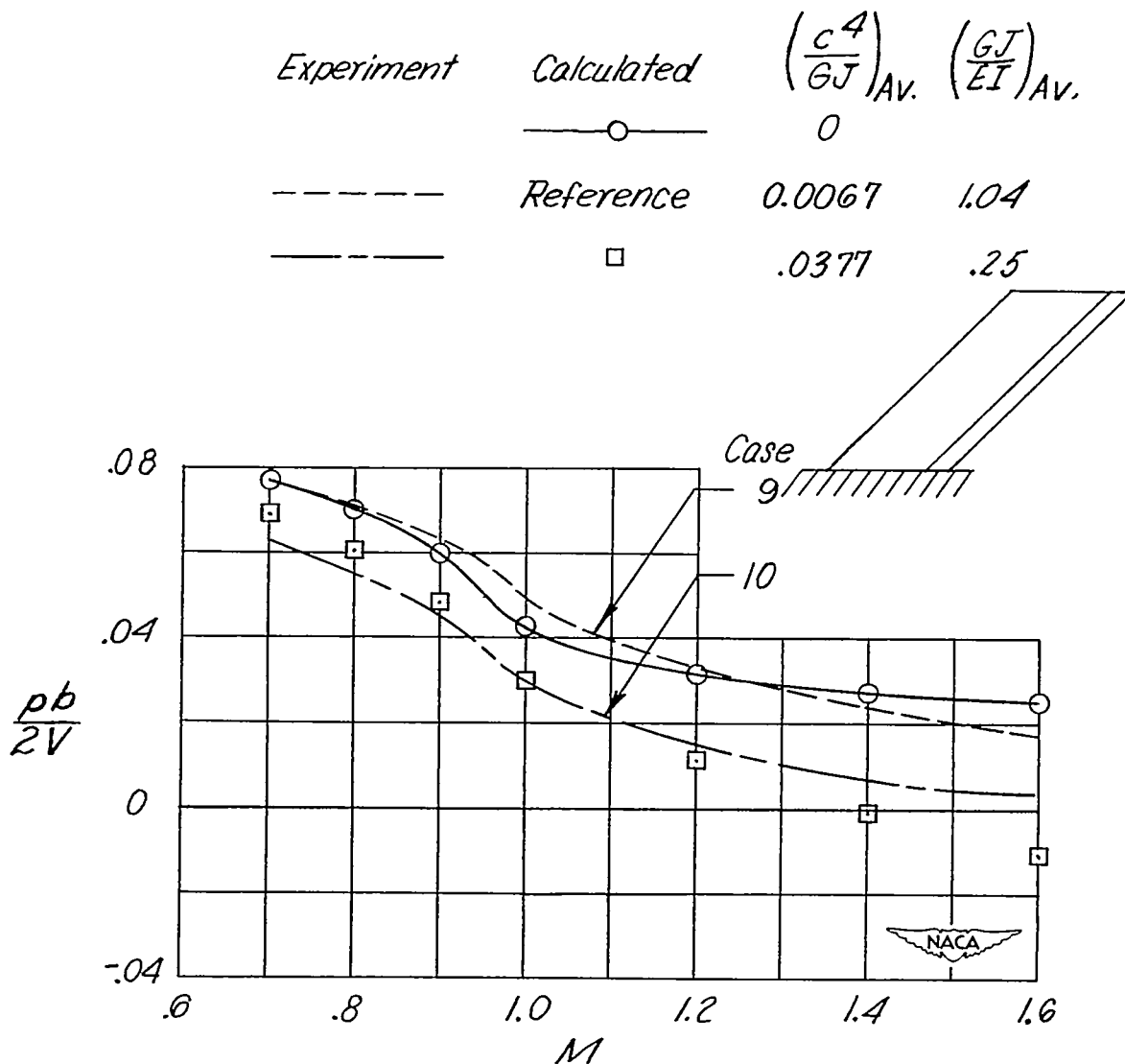


Figure 12.- Effect of decreasing wing stiffness on the variation of rolling effectiveness with Mach number. $AR = 3.7$; $\Lambda = 45^\circ$; $\lambda = 1.0$; $\delta_a = 5^\circ$; NACA 65A009 airfoil section; $k_1 = 0.19$; $k_0 = 1.0$.

CONFIDENTIAL

CONFIDENTIAL

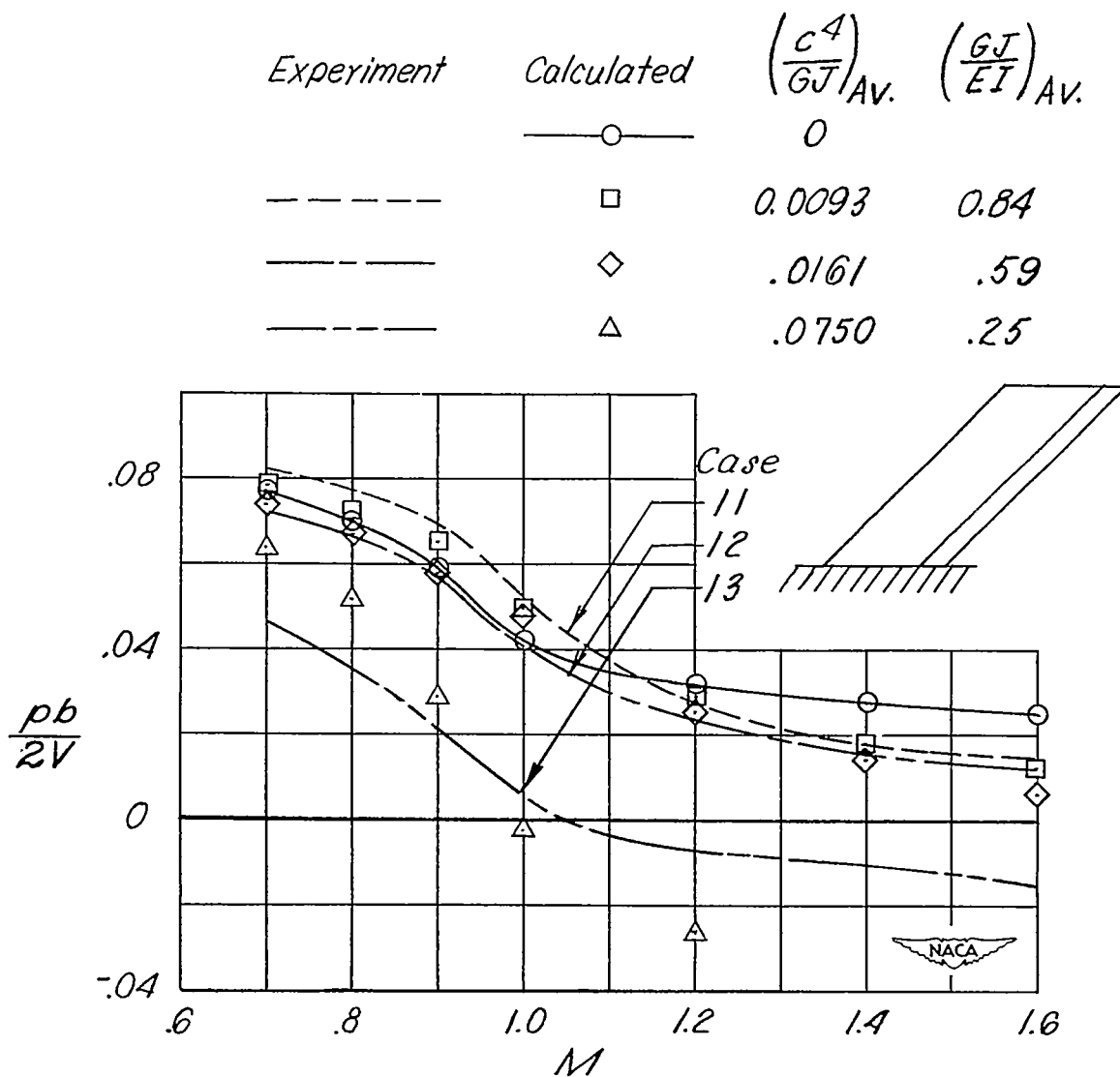


Figure 12.- Concluded.

CONFIDENTIAL

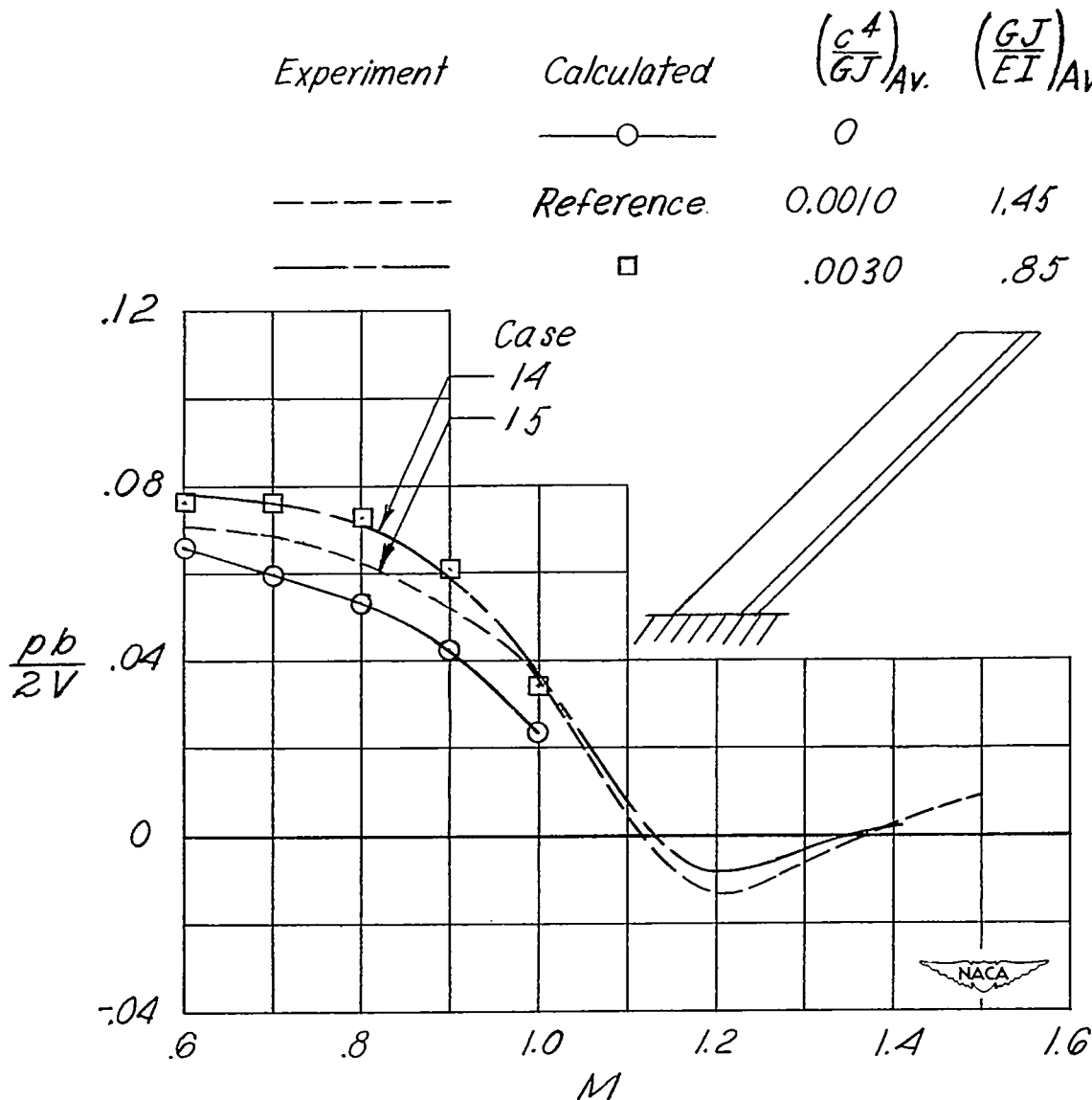
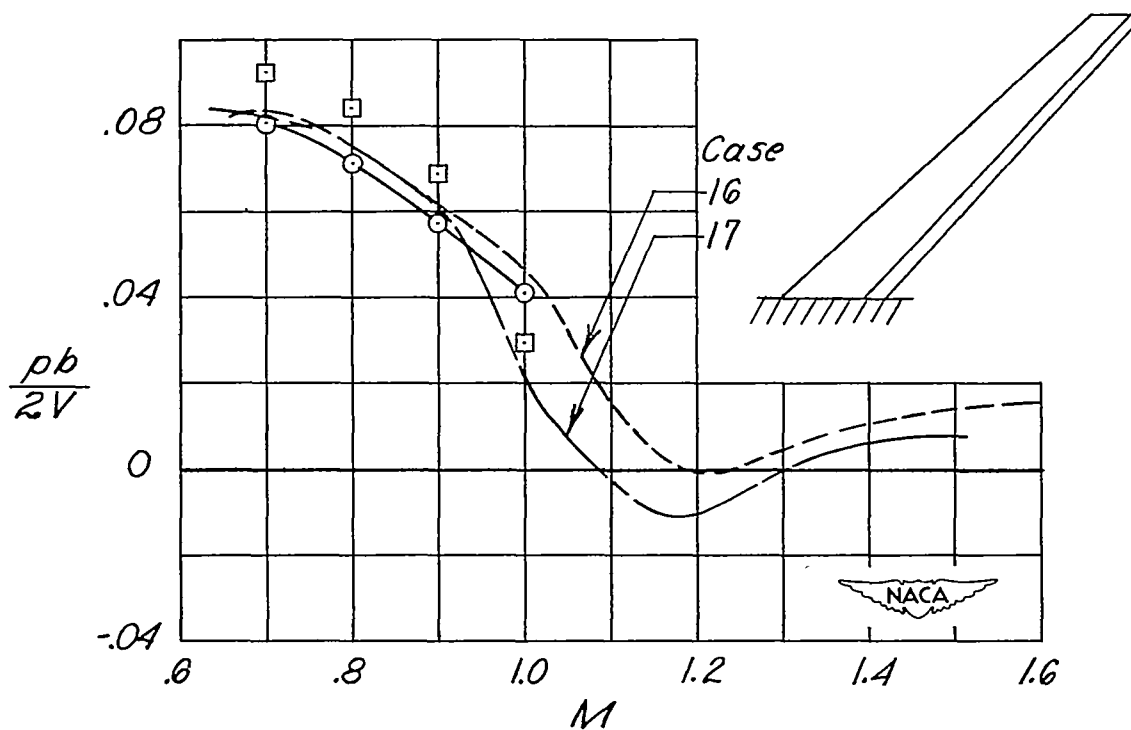
(a) $\lambda = 1.0$.

Figure 13.- Effect of decreasing wing stiffness on the variation of rolling effectiveness with Mach number. $AR = 8.0$; $\Lambda = 45^\circ$; NACA 65₁A012 airfoil section; $\delta_a = 5^\circ$; $k_1 = 0.13$; $k_0 = 1.0$.

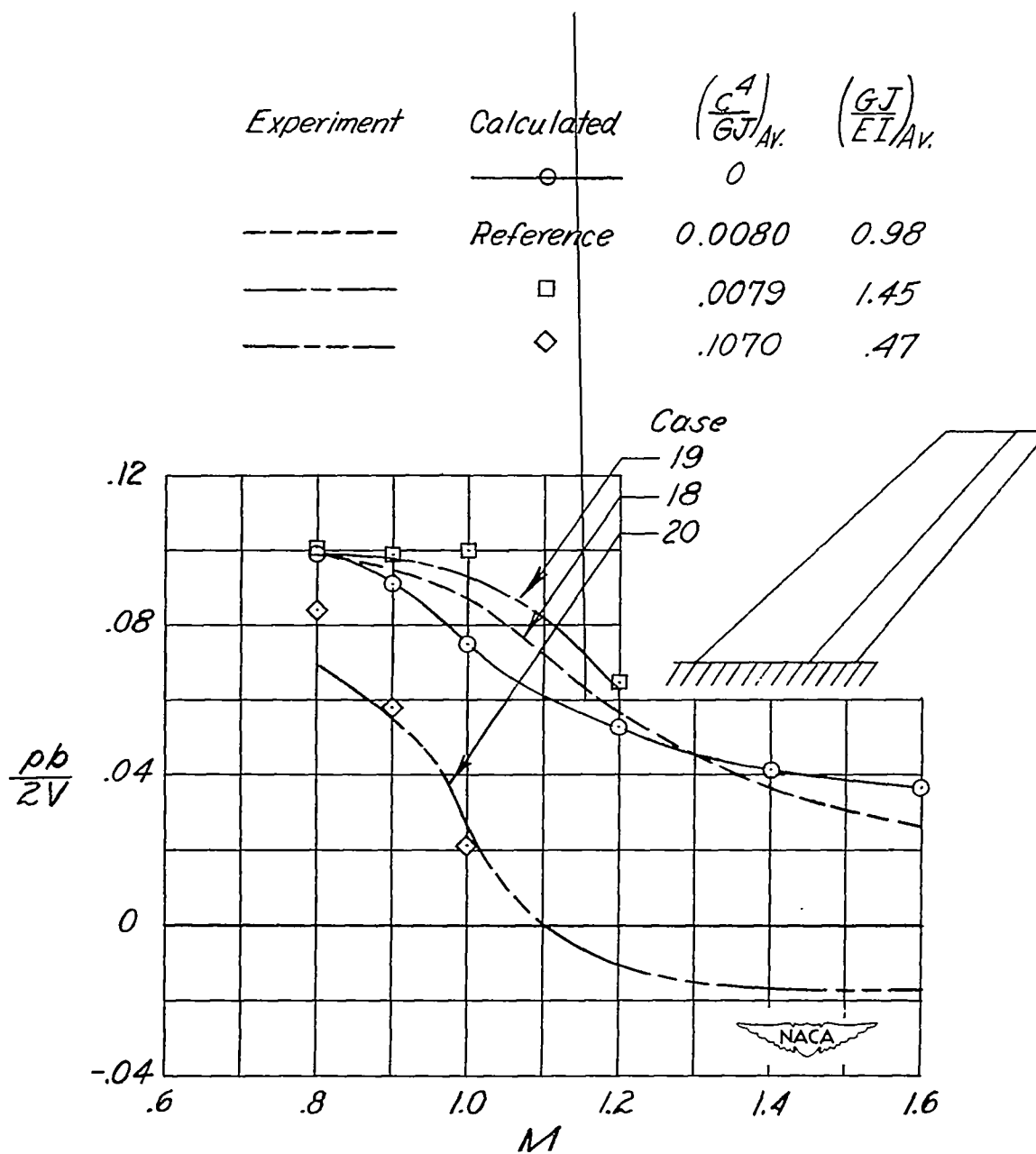
CONFIDENTIAL

Experiment	Calculated	$\left(\frac{c^4}{GJ}\right)_{Av.}$	$\left(\frac{GJ}{EI}\right)_{Av.}$
	—○—	0	
-----	Reference	0.0004	1.43
-----	□	.0030	.85



(b) $\lambda = 0.5$.

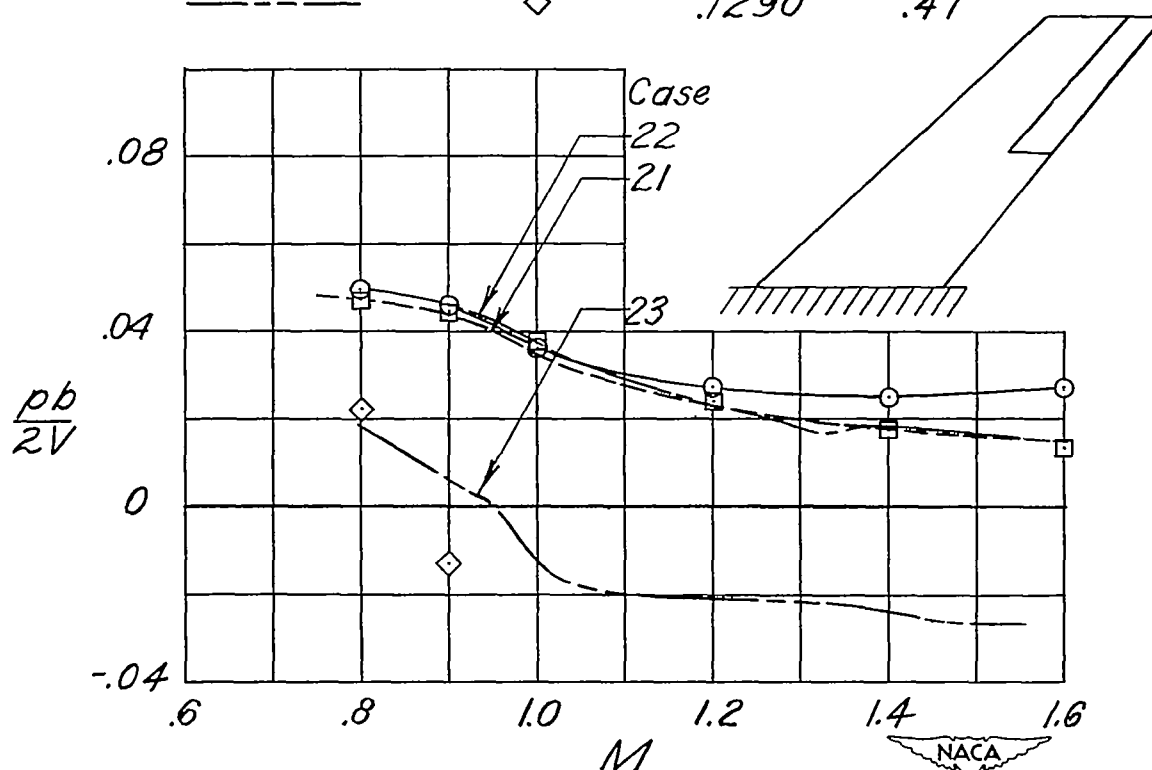
Figure 13.- Concluded.



(a) $k_1 = 0.14$; $k_0 = 1.0$.

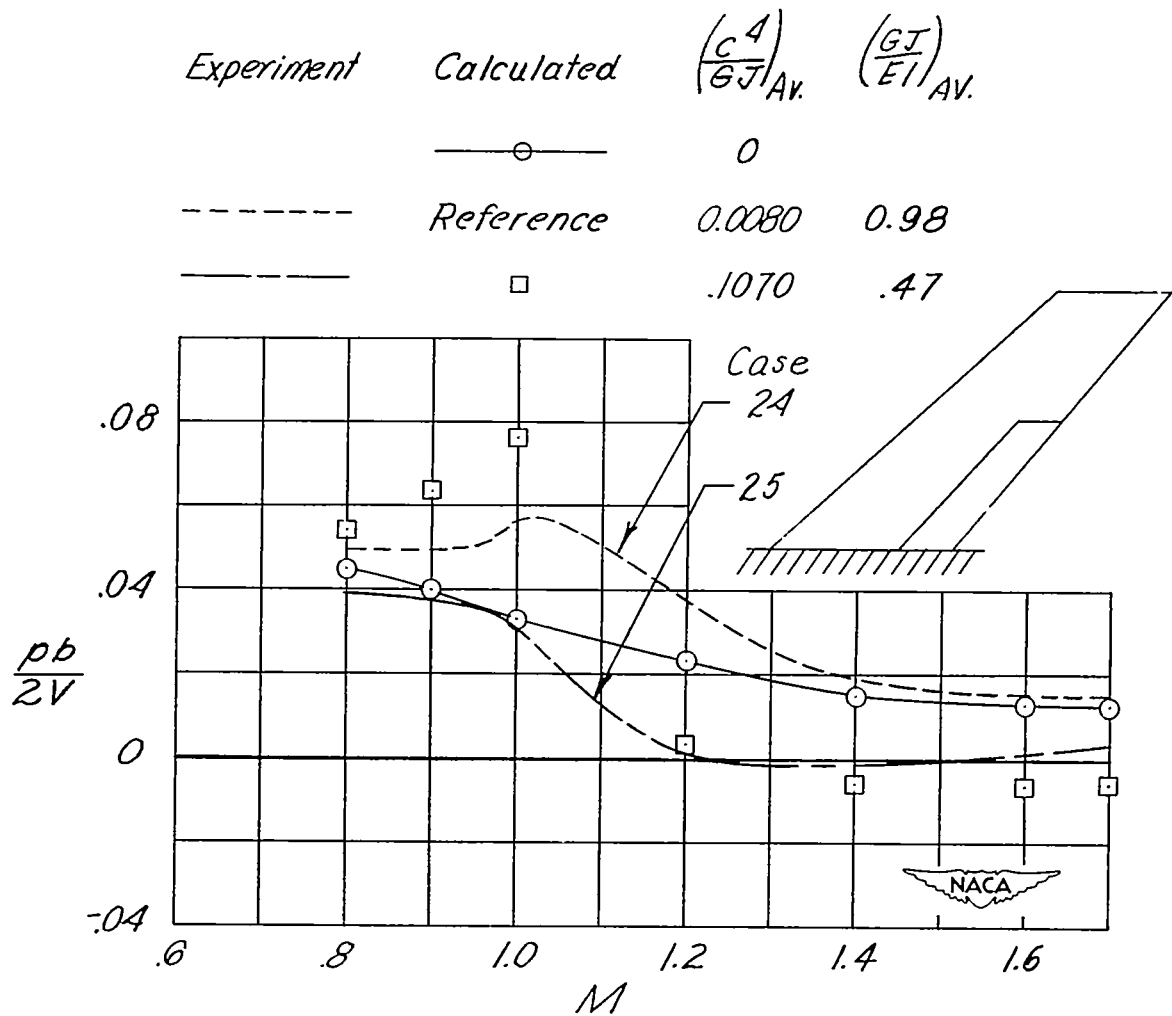
Figure 14.- Effect of decreasing wing stiffness on the variation of rolling effectiveness with Mach number. $AR = 4.0$; $\Lambda_c/4 = 45^\circ$; NACA 65A006 airfoil section; $\delta_a = 5^\circ$; $\frac{c_a}{c} = 0.3$; $\lambda = 0.6$.

Experiment	Calculated	$\left(\frac{c^4}{GJ}\right)_{Av.}$	$\left(\frac{GJ}{EI}\right)_{Av.}$
	—○—	0	
-----	Reference	0.0080	0.98
-----	□	.0079	1.45
-----	◇	.1290	.47



(b) $k_1 = 0.57$; $k_0 = 1.0$.

Figure 14.- Continued.



(c) $k_1 = 0.14$; $k_0 = 0.57$.

Figure 14.- Concluded.

Experiment	Calculated	$\left(\frac{c^4}{GJ}\right)_{Av.}$	$\left(\frac{GJ}{EI}\right)_{Av.}$
	—○—	0	
-----	Reference	0.0079	1.45
—□—		.1290	.46

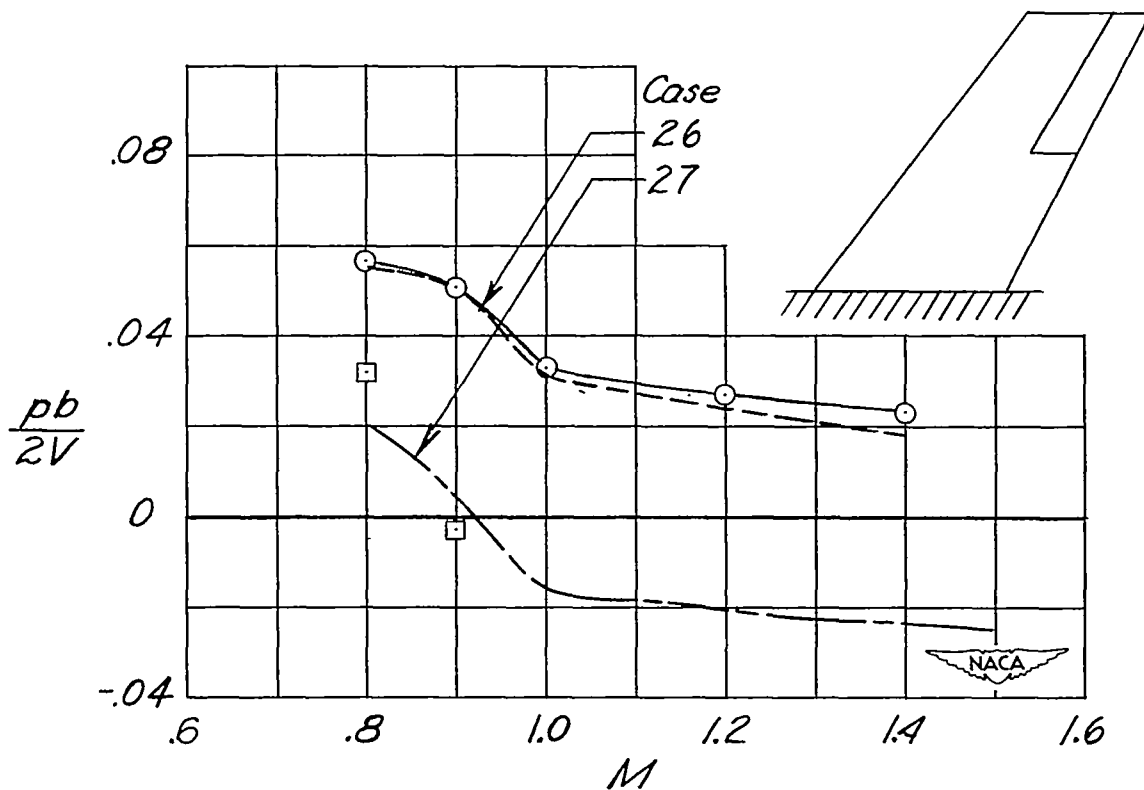


Figure 15.- Effect of decreasing wing stiffness on the variation of rolling effectiveness with Mach number. $AR = 4.0$; $\Lambda_c/4 = 35^\circ$; NACA 65A006 airfoil section; $\delta_a = 5^\circ$; $\frac{c_a}{c} = 0.3$; $\lambda = 0.6$; $k_1 = 0.57$; $k_0 = 1.0$.

CONFIDENTIAL

NACA RM L53H14

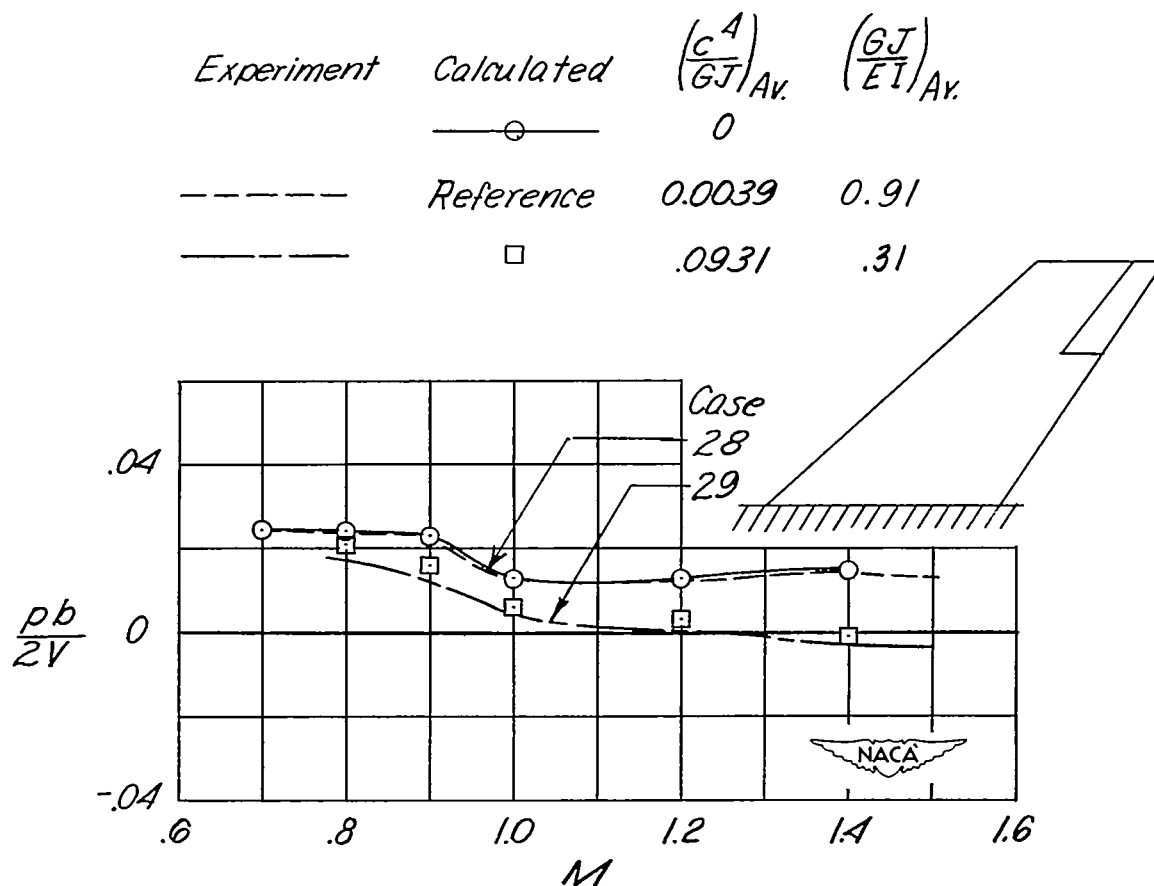
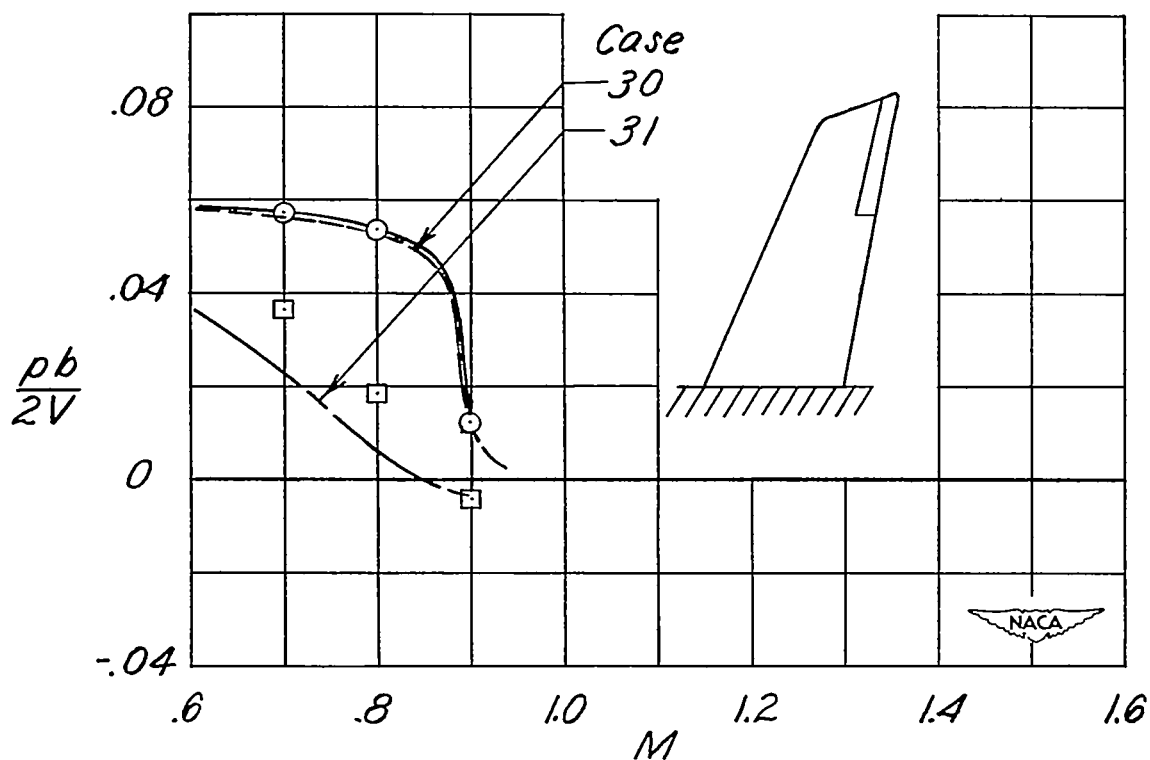


Figure 16.- Effect of decreasing wing stiffness on the variation of rolling effectiveness with Mach number. $AR = 3.0$; $\Lambda_c/4 \approx 45^\circ$; $\delta_a = 5^\circ$ (normal to hinge line) $k_1 = 0.678$; $k_0 = 1.0$; $\frac{c_a}{c} = 0.25$; NACA airfoil sections 0009-1.16 38/1.14 (modified) at the root, 0007-1.16 38/1.14 (modified) at the tip.

CONFIDENTIAL

Experiment	Calculated	$\left(\frac{c^4}{GJ}\right)_{Av.}$	$\left(\frac{GJ}{EI}\right)_{Av.}$
	—○—	0	
-----	Reference	0.0022	0.97
-----	□	.0423	1.29

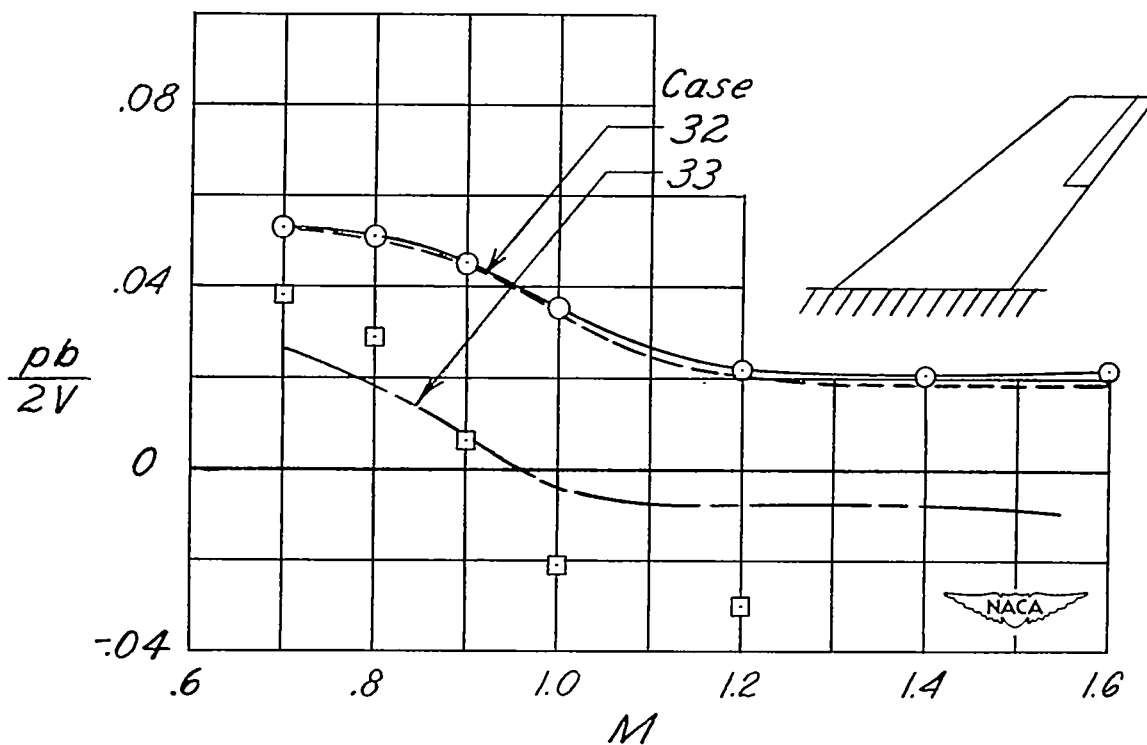


(a) $AR = 5.9$; $\Lambda_c/4 = 20^\circ$; $\lambda = 0.47$; $k_i = 0.70$; $k_o = 1.0$.

Figure 17.- Effect of decreasing wing stiffness on the variation of rolling effectiveness with Mach number. $\delta_a = 10^\circ$ (normal to hinge line); $\frac{c_a}{c} \approx 0.2$; NACA airfoil sections normal to 38-percent chord line (64-011 at root, 64-08.28 at tip).

CONFIDENTIAL

Experiment	Calculated	$\left(\frac{c^4}{GJ}\right)_{Av.}$	$\left(\frac{GJ}{EI}\right)_{Av.}$
	—○—	0	
-----	Reference	0.0047	1.00
-----	□	.0874	1.30



(b) $AR = 3.4$; $\Lambda_c/4 = 47.5^\circ$; $\lambda = 0.44$; $k_1 = 0.62$; $k_0 = 1.0$.

Figure 17.- Concluded.

CONFIDENTIAL

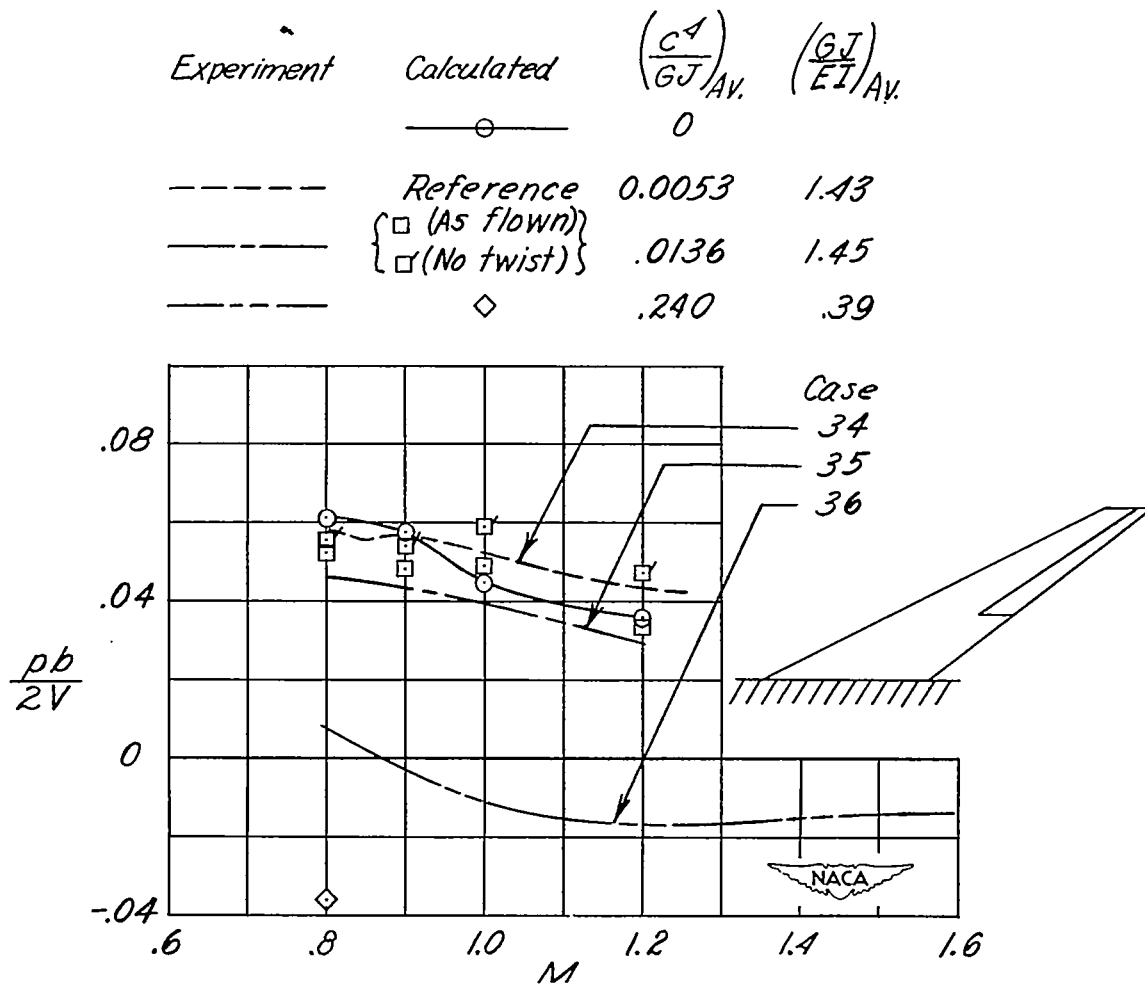


Figure 18.- Effect of decreasing wing stiffness on the variation of rolling effectiveness with Mach number. $AR = 3.5$; $\lambda = 0.25$; $\Lambda_c/4 = 61^\circ$; NACA 64A005 airfoil section; $\delta_a = 5^\circ$; $\frac{c_a}{c} = 0.3$; $k_1 = 0.5$; $k_0 = 1.0$.

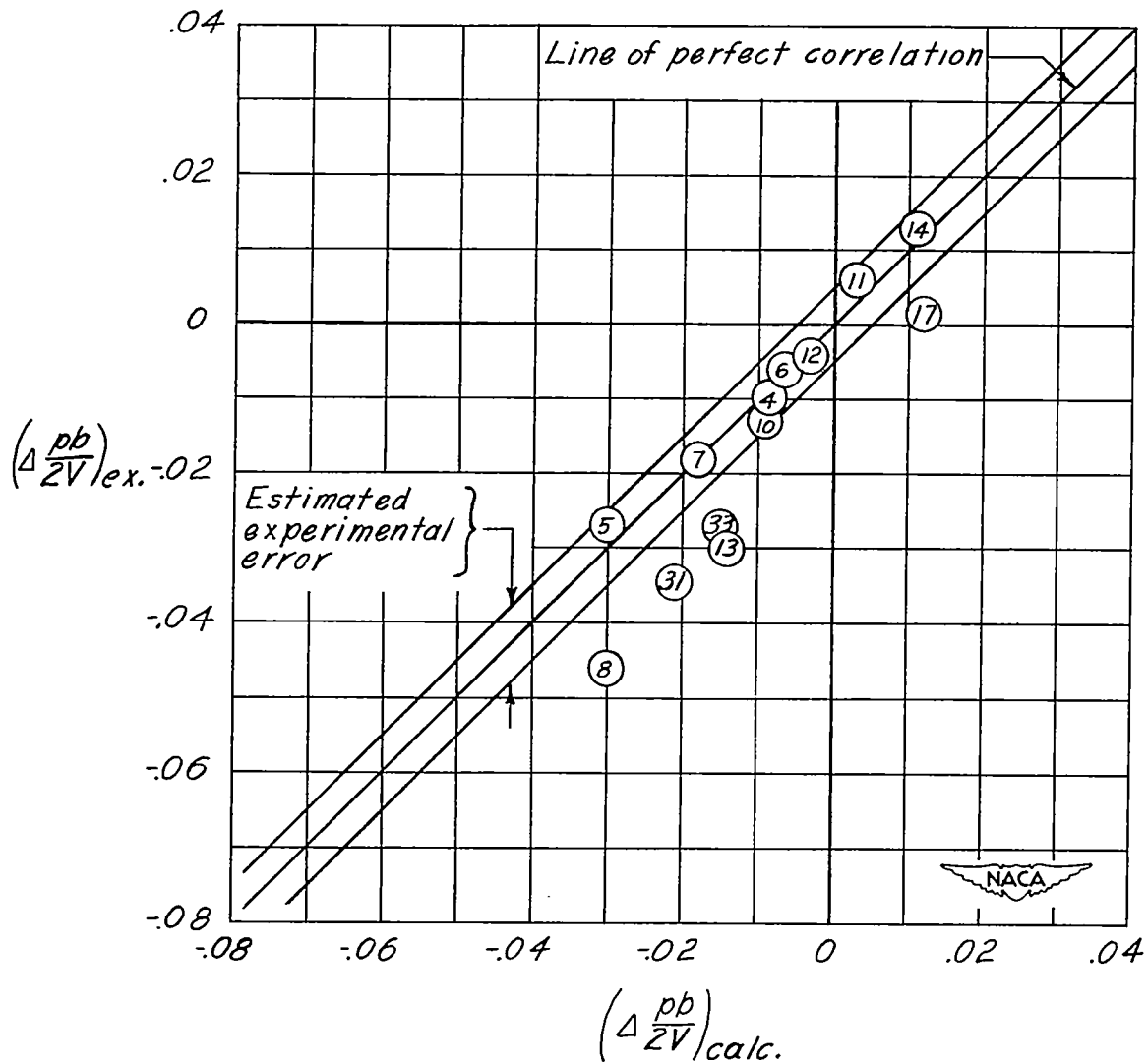
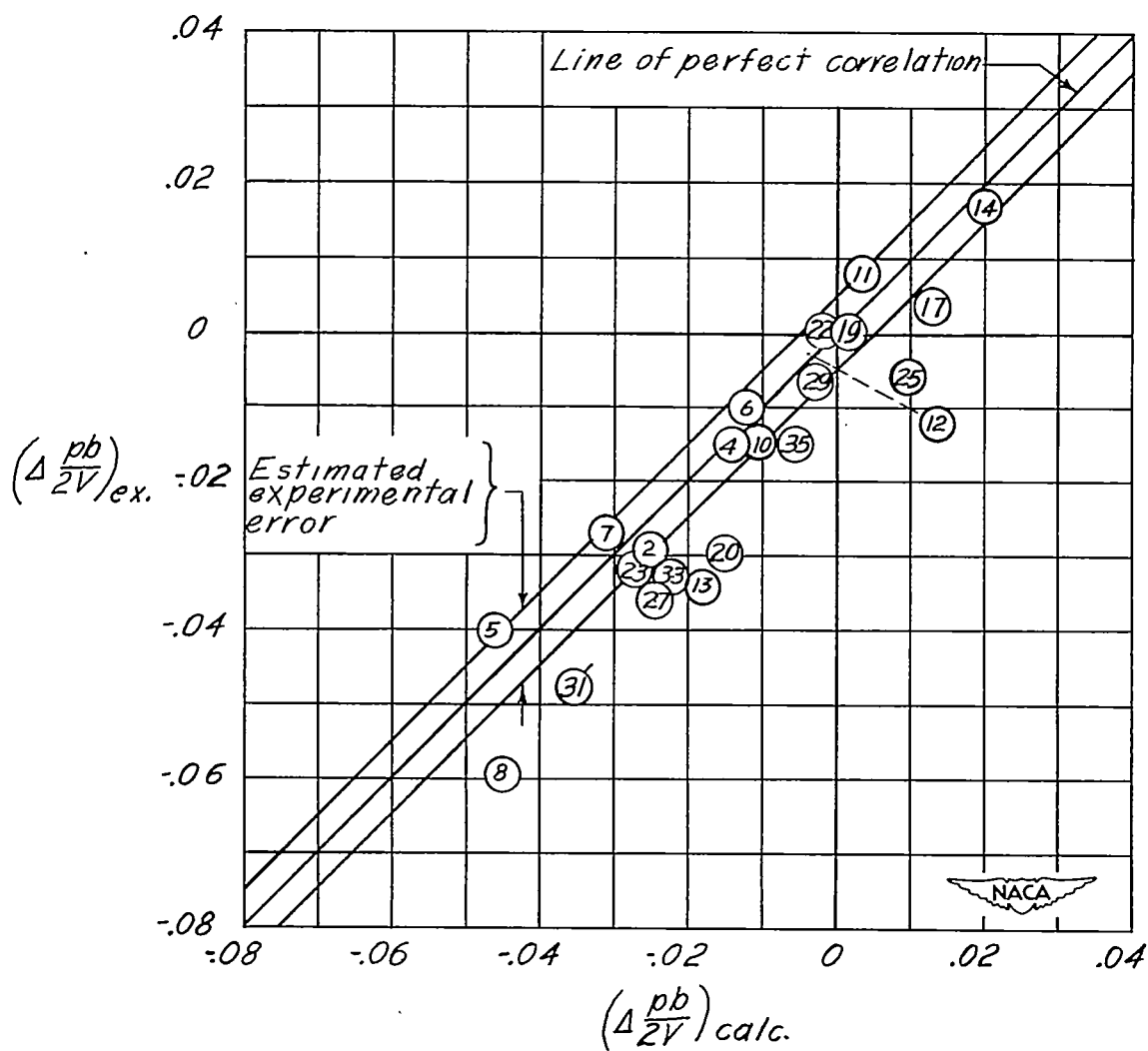
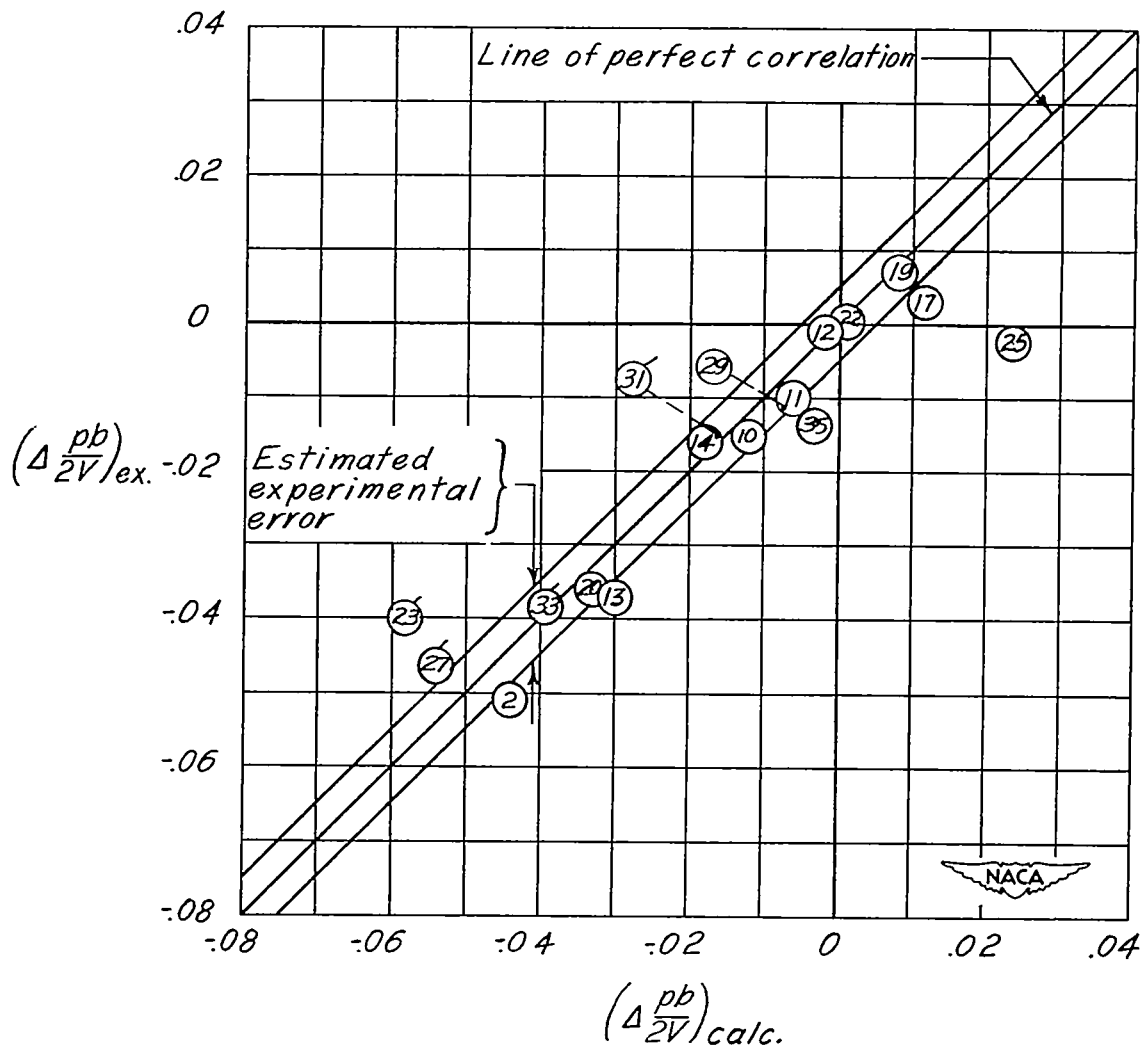
(a) $M = 0.7$.

Figure 19.- Comparison of the measured change in rolling effectiveness due to aeroelasticity with that calculated by means of the simplified method. Number inside symbol denotes test case.



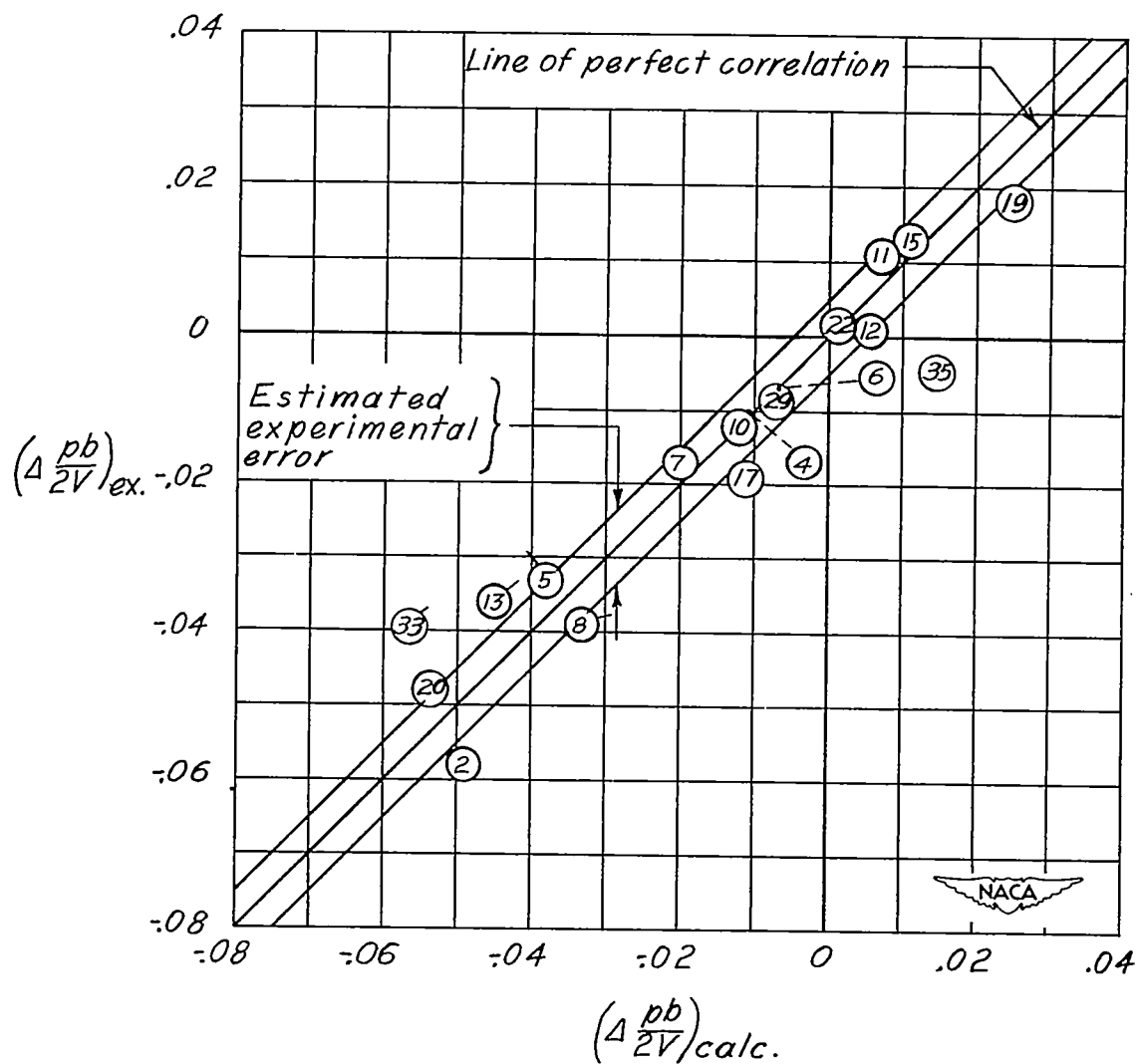
(b) $M = 0.8$. (Flagged symbol indicates that measured change in $pb/2V$ due to aeroelasticity ≥ 80 percent.)

Figure 19.- Continued.



(c) $M = 0.9$. (Flagged symbols indicate that measured change in $pb/2V$ due to aeroelasticity ≥ 80 percent.)

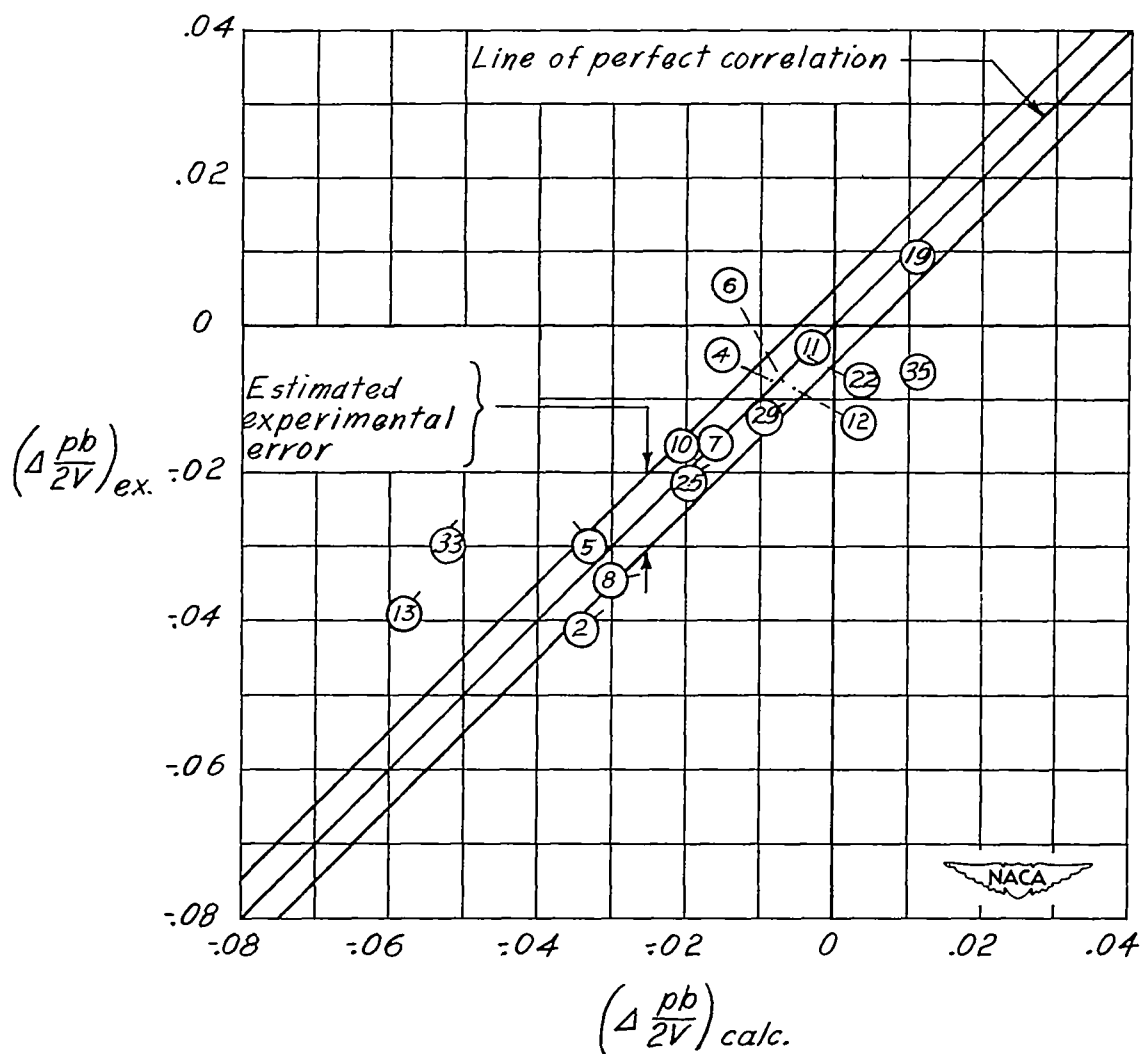
Figure 19.- Continued.



(d) $M = 1.0$. (Flagged symbols indicate that measured change in $pb/2V$ due to aeroelasticity ≥ 80 percent.)

Figure 19.- Continued.

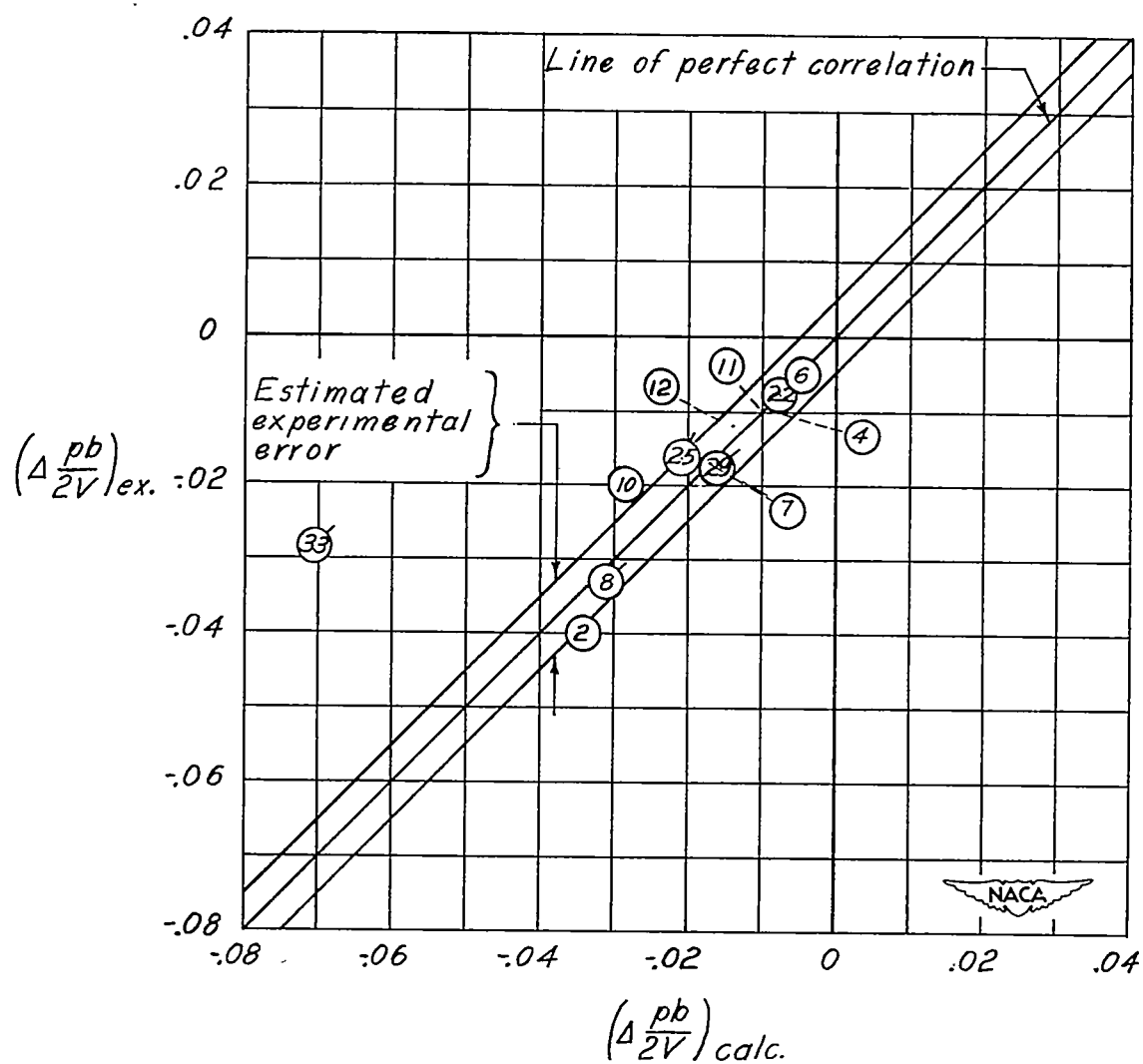
CONFIDENTIAL



(e) $M = 1.2$. (Flagged symbols indicate that measured change in $pb/2V$ due to aeroelasticity ≥ 80 percent.)

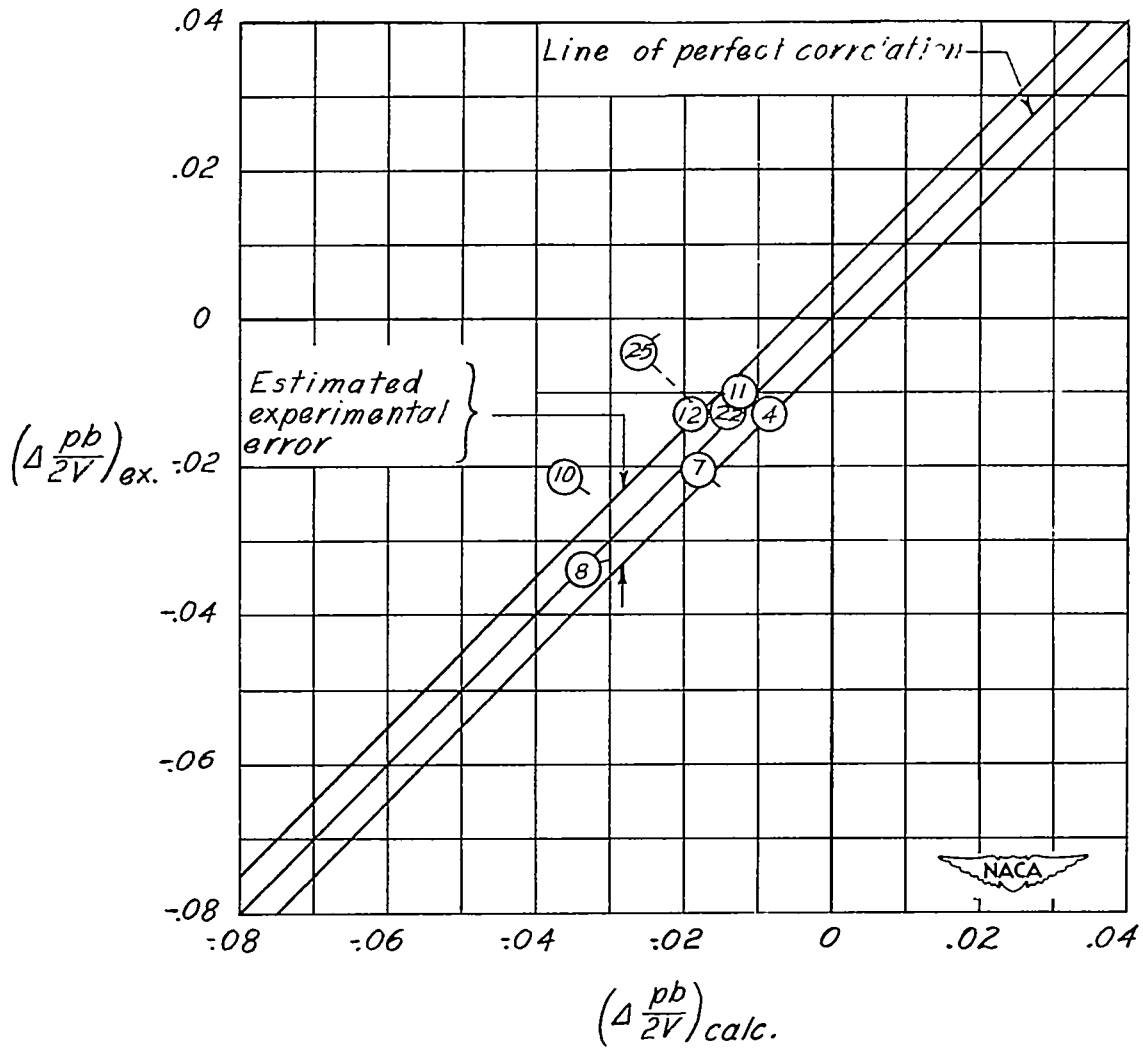
Figure 19.- Continued.

CONFIDENTIAL



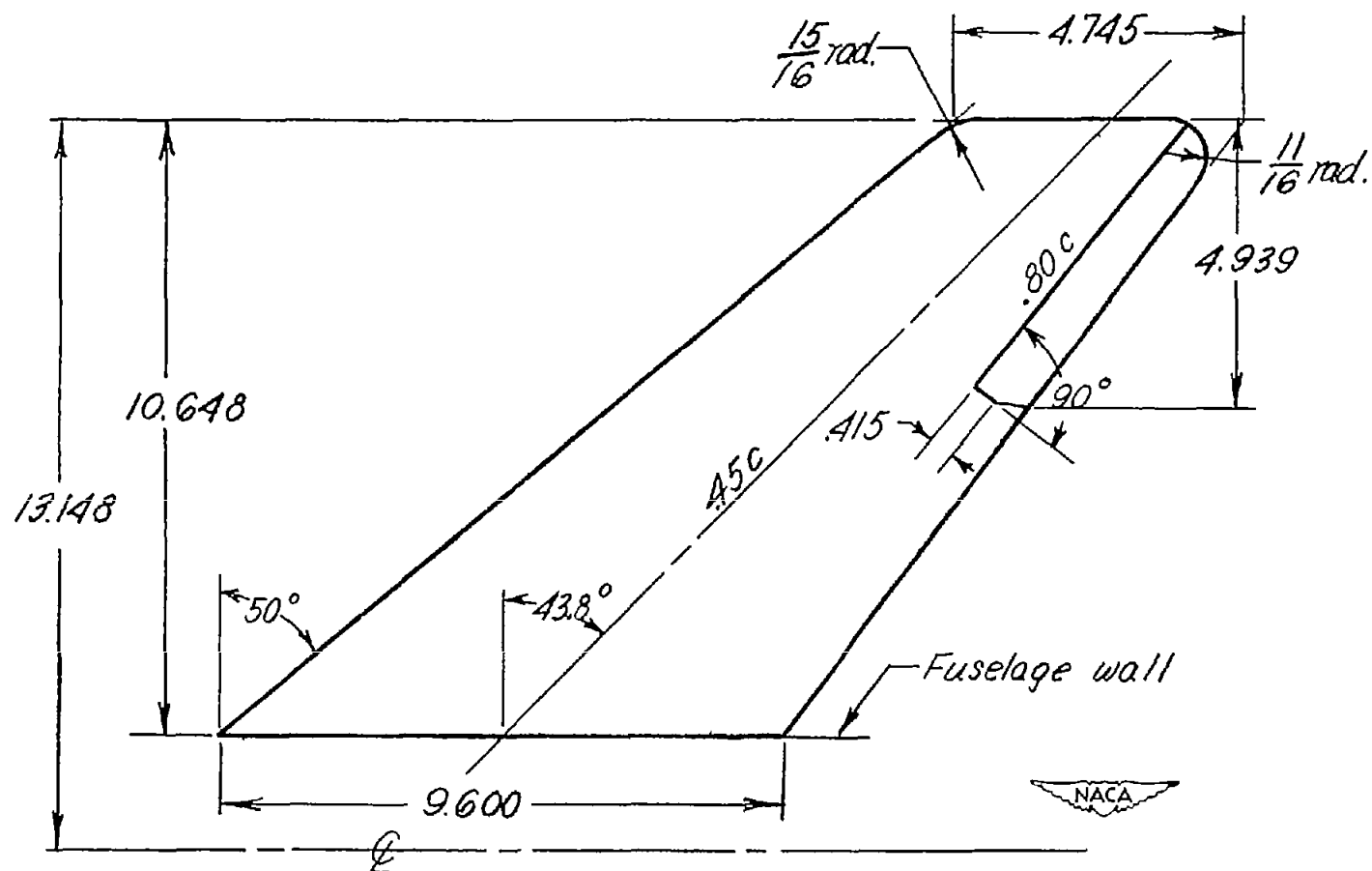
(f) $M = 1.4$. (Flagged symbols indicate that measured change in $pb/2V$ due to aeroelasticity ≥ 80 percent.)

Figure 19.- Continued.



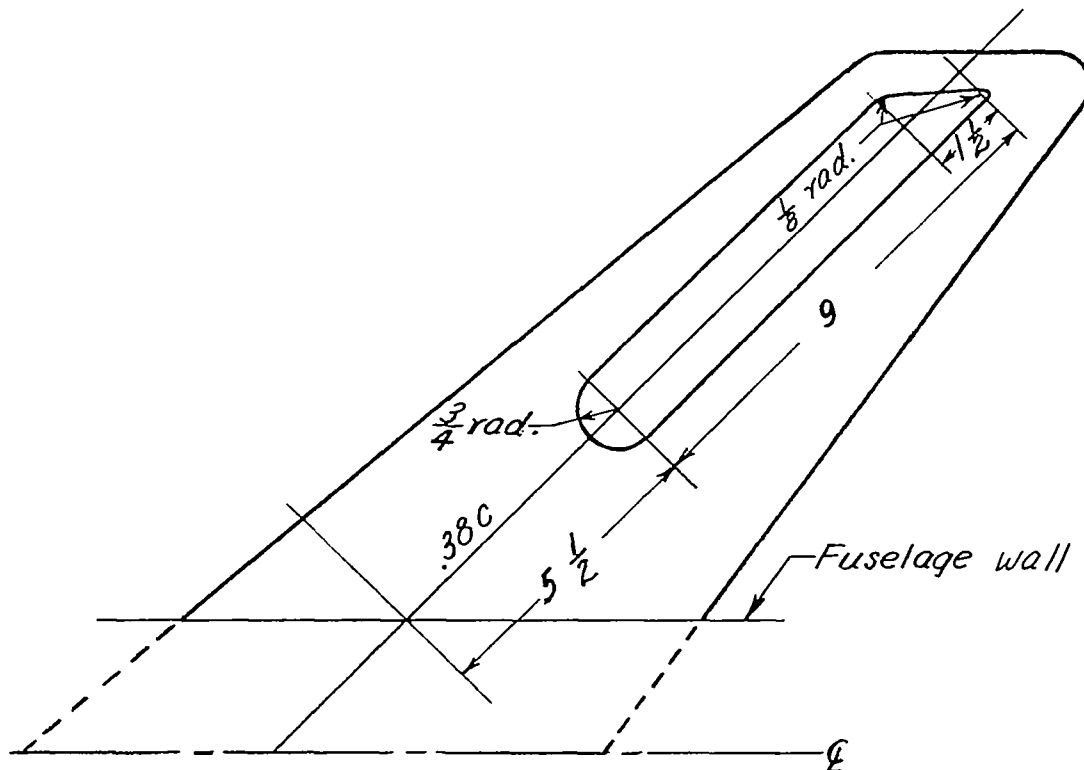
(g) $M = 1.6$. (Flagged symbols indicate that measured change in $pb/2V$ due to aeroelasticity ≥ 80 percent.)

Figure 19.- Concluded.

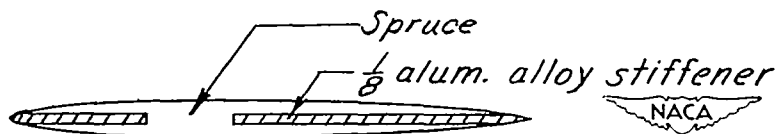


(a) External details.

Figure 20.- Description of example wings (case 33). Airfoil section is NACA 64-011 at the root, 64-08.28 at the tip normal to the 38-percent chord line. (All dimensions are in inches.)



(b) Details of chord-plane stiffener.



(c) Typical section (grain of wood approximately normal to model center line) - not to scale.

Figure 20.- Concluded.

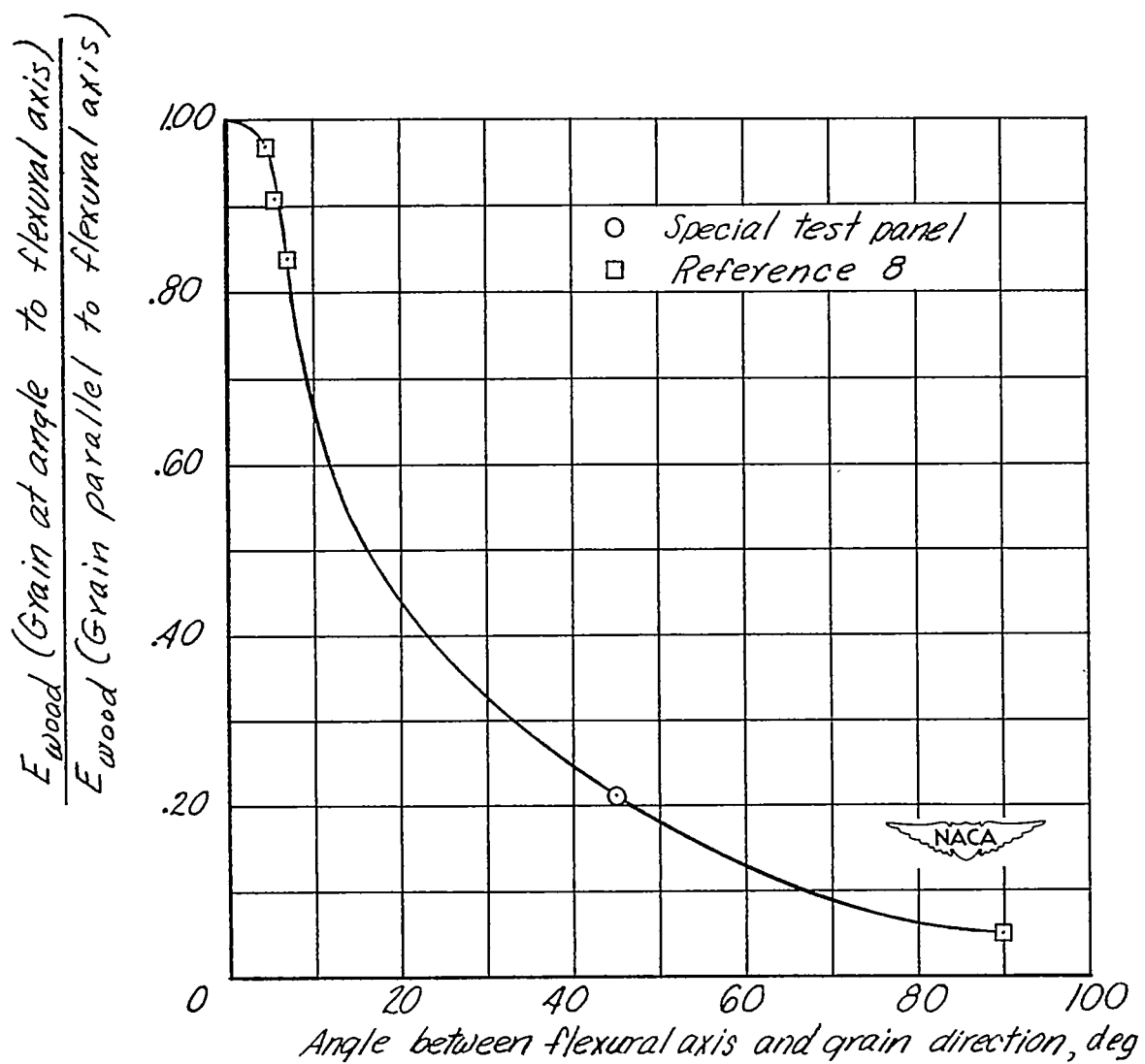


Figure 21.- Effect of grain orientation upon Young's modulus of elasticity for wood.

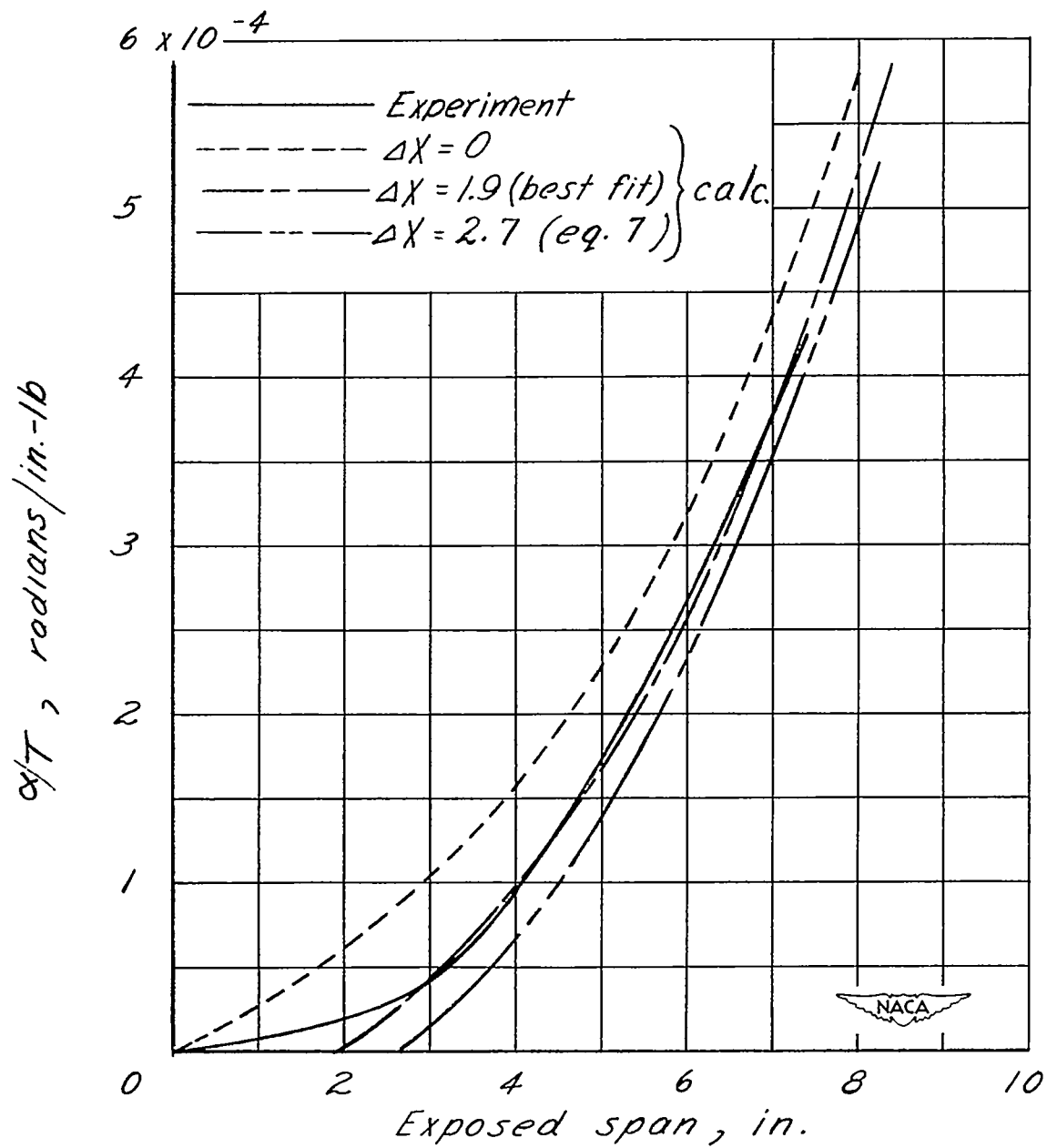


Figure 22.- Comparison of measured and calculated spanwise variation of wing twist.